Research Square

Preprints are preliminary reports that have not undergone peer review.
They should not be considered conclusive, used to inform clinical practice,
or referenced by the media as validated information.

SMNK-1 and VHA-18 are essential for FB-MO complex assembly and transport during spermatogenesis in C. elegans

Peng Wang

wangpeng615@mails.ucas.edu.cn

Institute of Biophysics, Chinese Academy of Sciences

Xiaojing Ma

College of Life Sciences, Beijing Normal University

Xinyan Chen

Institute of Biophysics, Chinese Academy of Sciences

Lianwan Chen

Institute of Biophysics, Chinese Academy of Sciences

Xiaolong Zhang

College of Life Sciences, Beijing Normal University

Ying Chen

College of Life Sciences, Beijing Normal University

Ning Wang

Institute of Biophysics, Chinese Academy of Sciences

Qiushi Wang

Institute of Biophysics, Chinese Academy of Sciences

Zheng Cao

Institute of Biophysics, Chinese Academy of Sciences

Yong Liu

College of Life Sciences, Fuyang Normal University

Yanmei Zhao

Institute of Biophysics, Chinese Academy of Sciences

Long Miao

Article

Keywords: Casein kinase, MSP assembly, v-ATPase, spermatogenesis, C. elegans

Posted Date: February 28th, 2025

DOI: https://doi.org/10.21203/rs.3.rs-6000630/v1

License: This work is licensed under a Creative Commons Attribution 4.0 International License.
Read Full License

Additional Declarations:
Table 1 is available in the Supplementary Files section.

There is **NO** Competing Interest.

Version of Record: A version of this preprint was published at Nature Communications on September 7th, 2026. See the published version at https://doi.org/10.1038/s41467-026-75577-6.

SMNK-1 and VHA-18 are essential for FB-MO complex assembly and transport during spermatogenesis in *C. elegans*

Authors

Xiaojing Ma[1,2,3,5], Xinyan Chen[2,5], Lianwan Chen[2,5], Peng Wang[2,3,5*], Xiaolong Zhang[1], Ying Chen[1], Ning Wang[1,2,3], Qiushi Wang[2], Zheng Cao[2], Yong Liu[4], Yanmei Zhao[2 *], Long Miao[1,2,3,4,6 *]

[1]MOE Key Laboratory of Cell Proliferation and Regulation Biology, College of Life Sciences, Beijing Normal University, Beijing 100875, China.

[2]Key Laboratory of RNA Biology, CAS Center for Excellence in Biomacromolecules, Institute of Biophysics, Chinese Academy of Sciences, Beijing 100101, China.

[3]University of Chinese Academy of Sciences, Beijing 100049, China.

[4] College of Life Sciences, Fuyang Normal University, Fuyang 236037, China

[5]These authors contributed equally to this work.

[6]Lead author

[*]Correspondence: lmiao@bnu.edu.cn (L.M.), ymzhao@genetics.ac.cn(Y.Z.), wangpeng615@mails.ucas.edu.cn (P.W.)

Keywords

Casein kinase, MSP assembly, v-ATPase, spermatogenesis, *C. elegans*

Abstract

The spatiotemporal control of asymmetric positioning of cellular cargoes such as macromolecules and organelles during spermatogenesis is essential to produce functional sperm in most animal species. Yet, the regulatory mechanisms that govern cargo sorting and transport remain largely unknown. Here we show that the casein-like kinase SMNK-1 localized on the surface of membranous organelle (MO) is required to recruit IDR-containing SPE-18 and facilitate the assembly of Major Sperm Protein (MSP) condensate, named Fibrous Body (FB) in spermatocyte during spermatogenesis in *C. elegans*. Meanwhile, the MO-localized VHA-18, the H subunit of the v-ATPase, is required for pumping the cytoplasmic protons into MOs, generating an alkaline cytoplasmic microenvironment adjacent to MOs, favorable for packaging MSP filaments into fibrous body (FB) and thus guaranteeing the correct cargo sorting during spermatogenesis. Thus, the interplay between membraneless condensate FBs mediated by SMNK-1 and membrane-bound organelle MOs regulated by VHA-18 provides a novel yet uncovered mechanism for cargo sorting and vectorial transport during spermatogenesis in *C. elegans*.

INTRODUCTION

Infertility has gradually become a significant global issue. It affects 12–15% of reproductive-aged couples worldwide, and male factor contributes to nearly half of infertility cases[1,2]. Therefore, it is crucial to understand sperm infertility. However, studies utilizing human sperm are challenging due to several reasons, such as the complexity of human-specific biological processes Several model organisms have been extensively employed in the study of male fertility and spermatogenesis. In *C. elegans*, it is easy to perform genetic and cell biology studies, which makes it a particularly valuable model in investigating sperm fertility. Unlike the spermatozoa in most animals, which typically have whip-like flagella composed of microtubules, amoeboid spermatozoon of *C. elegans* employs a single pseudopod filled with gel-like cytoskeletal meshwork composed of the major sperm protein (MSP) to facilitate the motility and migration. MSP, a 14 kDa basic protein, is exclusively expressed in nematode sperm, making up 15–20% of the total protein and 40% of the soluble protein in the sperm cell[3].

Two of the major reasons for sperm infertility are due to abnormal spermatogenesis and sperm activation. Spermatogenesis is a complex process that involves mitotic proliferation of spermatogonia, meiotic division of spermatocytes, and differentiation of haploid spermatids into mature spermatozoa[4]. During the sorting stage in meiosis II of spermatogenesis in *C. elegans,* the developing spermatid containing a haploid nucleus, some mitochondria, and Membranous Organelles (MOs) is budded away from the residual body (RB), where the unnecessary components such as the endoplasmic reticulum, ribosomes, tubulin, actin are disposed[5]. The MOs, originated from the Golgi complexes in the spermatocyte, are initially observed during the pachytene stage of meiosis I. Subsequently, MSP is polymerized into filaments, which are hexagonally packed and encased by the membrane of the MOs, forming the MO-associated fibrous body (FB) complex, named as FB-MO

complex. The sequestrated MSP remains in these FBs through the post-meiotic partitioning process, during which FB-MOs complexes partition vectorially to individual spermatids. The FB–MOs assist in transporting MSP and other components into spermatids[6,7]. Once spermatids bud off the RB, the membrane surrounding the FBs retracts, and then the FBs disassemble into the cytoplasm[3]. During spermatid activation, the MOs docked underneath the plasma membrane (PM) fuse with PM, releasing their contents, and the cell polarizes to extend a single pseudopod powered by the cycled assembly/disassembly of MSP cytoskeleon[8]. Therefore, the assembly of MSP into membraneless condensate FBs associated with MOs in spermatocyte helps sort MSP into the developing haploid spermatids during budding, guaranteeing that MSPs are transported into spermatids, instead of the RB.

However, little is known about the composition of FBs, such as accessory proteins, helping to mediate MSP assembly and MSP-mediated motility. Additionally, the underlying mechanisms for selective cargo sorting and transport during spermatogenesis remain largely unknown. In this study, we identified a sperm-specific and MO-associated casein-like kinase gene SMNK-1 and found that it is necessary for FB assembly during spermatogenesis in *C. elegans*. Either null allele or kinase-dead *smnk-1* sperm are defective in activation and motility acquisition, thus both hermaphrodites and males of *smnk-1* mutant are sterile. We showed that the SMNK-1, localized to the MOs' surface in the early stage of spermatocytes, was essential for recruiting SPE-18 (an IDR-containing protein necessary for MSP filament bundling) and initiating FB assembly. Furthermore, we discovered that the H subunit of v-ATPase, localized on MOs, played a pivotal role in maintaining MOs morphology and function, and provided an alkaline cytoplasmic microenvironment favorable for the assembly of MSP filaments into FBs.

RESULTS

SMNK-1 is required for fertility in both hermaphrodites and males

To identify genes that are crucial for spermatogenesis, we screened the gene expression profiles focusing on spermatogenesis in *C. elegans*. [12–14] We found C09B9.4 and named it as *smnk-1* (Spermatogenetic MSP Nucleation Kinase-1) based on its function. The RT-PCR results showed that *smnk-1* was highly expressed in sperm-producing *fem-3(q96 gf)* worms when compared to the mRNA expression level of oocytes-producing *fem-1(hc17 lf)* and germline-deficient *glp-4* worms (Figs. 1A and 1B). Therefore, the protein encoded by *smnk-1* might be involved in spermatogenesis.

SMNK-1, like SPE-6, is a member of the greatly expanded *C. elegans* casein kinase 1 superfamily (CK1), with 78 genes in *C. elegans* versus 12 in human. Many of these genes are expressed in a spermatogenesis-enriched manner and may be functionally redundant[15,16]. Sequence analysis showed that SMNK-1 lacks transmembrane domain and a signal peptide, indicating that SMNK-1 is a cytoplasmic protein. BLASTP analysis identified two highly conserved homologs of SMNK-1 in the *Caenorhabditis* genus (Supplementary Fig.1A). SMNK-1 protein contains 359 amino acids, with a conserved ser/thr kinase catalytic domain and a flexible C-terminal tail. In most kinases, the activation-loop, beginning with the residues DFG in the catalytic domain, undergoes a conformational change upon phosphorylation of Ser, Thr or Tyr residues within the loop, which makes both ATP and substrates accessible for the active site. Sequence alignment of *smnk-1* with *ck1s* in other species identified a conserved Thr195 in the activation loop of SMNK-1 (Supplementary Fig.1A).

Using the CRISPR-Cas9 genome editing system, we generated a frameshift mutation allele *ibp107*, which has 7 bases insertion in the first exon of *smnk-1* gene (Figs. 1C and Supplementary Fig.1B). We tested whether the mutation affected the worm fertility. Each control hermaphrodite could produce more than

200 progenies, while each *smnk-1(ibp107)* hermaphrodite only produced about 10 progenies, making them nearly sterile. The infertility of *smnk-1(ibp107)* hermaphrodites can be rescued by mating them with *him-5* males, which supply normal sperm (Fig. 1D). This indicates that the infertility in *smnk-1(ibp107)* hermaphrodites is due to their defective sperm. Besides, obvious unfertilized oocytes were observed on the plates of *smnk-1(ibp107);him-5* hermaphrodites (Supplementary Fig.1C). These findings imply that SMNK-1 may have a sperm-specific function in hermaphrodites. Furthermore, *smnk-1(ibp107)* is not a temperature-sensitive strain because the fertility of *smnk-1* hermaphrodites showed no difference at 16℃, 20℃ and 25℃ (Supplementary Fig.1D).

To test the male fertility, males were mated with the self-sterile *spe-8;dpy-4* hermaphrodites. The *spe-8* hermaphrodites are infertile due to the abnormality of their sperm activation[17]. However, their self-sterility can be rescued by mating them with males because of the trans-activation of *spe-8;dpy-4* hermaphrodite sperm by protease TRY-5 in the seminal fluid from males[18]. The *dpy-4* is a recessive mutant used to distinguish between cross-progeny and self-progeny[19]. Male sperm have a competitive advantage over hermaphrodite sperm[20–22,22]. Most progeny would be cross-progeny and exhibit a non-dumpy phenotype when WT male sperm are used after mating. Only when the sperm from males are used up or defective, trans-activated hermaphrodite sperm would be used to produce self-progeny, exhibiting a dumpy phenotype. When the control *him-5* males were used to mate with *spe-8;dpy-4* hermaphrodites, the majority of progeny were cross-progeny (non-dumpy); however, when the *smnk-1(ibp107);him-5* males were used for mating with *spe-8;dpy-4* hermaphrodites, almost all progeny were self-progeny (dumpy) (Fig. 1E), indicating a severe sperm defect in *smnk-1(ibp107)* males.

We also generated two other alleles, *ibp129,* in which the conserved residue T195 in the kinase activation loop is replaced with A, and *ibp116,* with a deletion of the C-terminal tail (Figs. 1C and S1B). We found that their fertility showed no

significant difference compared to the *ibp107* allele in both sexes (Figs. 1D and 1E). Therefore, the loss or inactivation of SMNK-1 significantly reduces the offspring counts due to sperm defects.

Then, we analyzed the motility of sperm ejaculated by *smnk-1* males into the hermaphrodite reproductive tract. The males stained with MitoTracker Red (a dye that labels mitochondria in live cells) were mated with non-labeled N2 hermaphrodites. After mating, MitoTracker Red-stained sperm from males were transferred to hermaphrodites and became activated. The sperm from control males (*him-5*) had the ability to crawl toward and accumulated in the spermatheca or the adjacent zones to prepare for fertilization. In contrast, the sperm from *smnk-1; him-5* males remained dispersed near the vulva (Fig. 1F), indicating that sperm from *smnk-1; him-5* are defective in motility. Together, these data demonstrate that SMNK-1 is required for fertility in both hermaphrodites and males and that the loss of SMNK-1 results in sperm-specific defects such as sperm motility and/or migration after ejaculation.

SMNK-1 is required for sperm activation during spermiogenesis

To determine how the *smnk-1* mutation affects sperm function, we crossed *smnk-1*(*ibp107*); *him-5* with the worm expressing *gfp::nkb-2* and H2B::mCherry to detect spermatogenesis and sperm activation in vivo. NKB-2 is the β subunit of Na^+/K^+ ATPase that is uniformly localized on the PM of spermatocytes and inactivated spermatids[23]. During sperm activation, the MOs fuse with the PM, trapping NKB-2 into the fused MOs and displaying as puncta on the side of cell body[23]. H2B tagged with mCherry indicating the nucleus is a component of histone. In hermaphrodites, no obvious difference was observed before the first ovulation (Supplementary Fig.2A). After ovulation, hermaphrodite sperm were pushed into and activated in the spermatheca. In the control, the GFP::NKB-2 would display as bright green puncta in spermatozoa located in the spermatheca. In *smnk-1* mutants, the fluorescence intensity of GFP::NKB-2 puncta in spermatozoa appeared reduced (Fig. 2A), indicating that the MO

fusion with PM might be affected during sperm activation in vivo in hermaphrodites.

We checked spermatogenesis by observing the distribution of GFP::NKB-2 in males. No obvious difference was observed in the fluorescence pattern of GFP::NKB-2 in spermatocytes and spermatids (Supplementary Fig.2B), indicating that *smnk-1* mutation does not cause any apparent defect in male germline development. Subsequently, we investigated spermiogenesis in vivo by using *swm-1* mutant males, which would undergo precocious activation due to the loss of an activation inhibitory signal[19]. We performed a time-lapse analysis and observed early activated motile spermatozoa with punctate GFP::NKB-2 fluorescence in the seminal vesicle of control *swm-1;him-5* males (Video S1). However, In *smnk-1;swm-1;him-5* males, the incompletely activated sperm with polarized GFP::NKB-2 puncta remained still in the seminal vesicle (Video S2). After dissecting the sperm from the aforementioned males, we observed obvious pseudopod formation and fully polarized GFP::NKB-2 puncta in the sperm from control *swm-1;him-5,* but not from the *smnk-1;swm-1;him-5* group (Fig. 2B). This indicates that the *smnk-1* mutation affects sperm activation and motility in vivo.

We isolated spermatids from the male seminal vesicle and treated them with artificial sperm activators, such as weak base NH_4Cl, TEA, proton carrier monensin, the microelement Zn^{2+}, and Pronase (Fig. 2C). FM1-43, a non-permeable membrane dye, was used to indicate the PM or the fused MOs because the fusion pores allow the entry of the dye into the permanent invaginations to stain the body of MOs. The *him-5* sperm were responsive to these extracellular activators, displaying a pseudopod and several fused MOs in the cell body side. However, *smnk-1;him-5* sperm failed to fully activate, with less fused MOs and almost no pseudopod formation (Fig. 2C). All the treatments with these in vitro activators in *smnk-1;him-5* mutant result in the similar phenotype (Fig. 2C). Taken together, these evidences suggest that

smnk-1 mutant sperm are defective in the fusion of MO with PM and pseudopod extension during sperm activation.

To further distinguish whether SMNK-1 affects the quantity of MOs in spermatogenesis or just the fusion of MO during sperm activation, the acidic MOs were labeled with LysoTracker Red[24]. We found that the number of MOs was normal in *smnk-1;him-5* sperm when compared with that from *him-5* control (Figs. 2D and 2E). However, when sperm were activated with Pronase, the number of fused MOs in *smnk-1;him-5* sperm decreased significantly and sperm kept round in shape, unlike the *him-5* spermatozoa with a long single pseudopod with significantly more fused MOs in the cell body (Figs. 2F and 2G). Taken together, these data demonstrate that SMNK-1 is required for sperm activation both in vivo and in vitro and that the loss of SMNK-1 would affect MO fusion and polarity establishment to form a single pseudopod during spermiogenesis.

smnk-1 mutants produce spermatocytes without FBs assembly

The failure of pseudopod formation in *smnk-1* sperm during activation could be due to the defects in MSP cytoskeleton assembly or sorting of FBs into spermatids during spermatogenesis. To test this hypothesis, we performed immunofluorescence microscopy (IFM) assay using anti-MSP monoclonal antibody. We found the MSP level in *smnk-1(ibp107)* spermatids was significantly lower than that in control group (Figs. 3A and Fig. 3B). Then we checked the MSP distribution in spermatocytes and found that there was no MSP assembly into FB in *smnk-1(ibp107)* spermatocytes. Instead, the MSP in *smnk-1(ibp107)* spermatocytes was completely dispersed in the cytoplasm without any aggregation. During the budding stage, part of the MSP was retained in the RB (Fig. 3C). Additionally, *smnk-1(ibp129) or smnk-1(ibp116)* allele also affected the FB assembly in spermatocyte (Figs. 3D and 3E), indicating that the kinase activity of SMNK-1 is necessary for MSP assembly into FBs in spermatocyte.

We then analyzed the ultrastructure of spermatocytes using transmission electron microscopy (TEM). MSP filaments were neatly arranged as FB and semi-surrounded by the tubule-like MO in WT spermatocytes. However, we observed that the tubule-like MOs contained less or no inclusions in *smnk-1* mutant spermatocytes (Fig. 3F). During meiotic division, some MO-like structures were lagged to RB in *smnk-1* mutant, implying that the disrupting membraneless FB assembly might indirectly cause the membrane-bound MOs to be delivered to the incorrect destination (Fig. 3G). Furthermore, we also compared the mRNA level of MSP in *smnk-1;him-5* with that in the *him-5* group, and found no significant difference between them (Supplementary Fig.3A). Therefore, we conclude that *smnk-1* mutants produce spermatocytes without FBs formation. Much less or even no MSP could be partitioned into spermatids when sperm cells bud off the RB, this fact is consistent with the above phenotype that sperm failed to extend pseudopod during sperm activation.

SMNK-1 is recruited to the MO surface to initiate FB assembly

Male gonad undergoes a developmental process from distal to proximal arm. The mitosis takes place in the distal region, followed by entry into meiosis after passing through the transition zone. During the meiosis, a prolonged pachytene occurs, characterized by chromosomal recombination and extensive gene expression related to spermatogenesis. Subsequently, the nucleus condenses into a distinct entity characterized by the significantly inhibited transcription. This is followed by a brief and rapid meiotic division stage, leading to the formation of spermatids. We could distinguish the various stages by the nuclear morphology revealed by Hoechst staining (Fig. 4A). Employing CRISPR-Cas9-based genome editing, we generated a GFP-tagged variant of *smnk-1*. The sperm-specific distribution pattern of SMNK-1::GFP fluorescence was observed at the proximal terminal of germline in males and at the spermatheca where sperm are stored in hermaphrodites (Supplementary Fig.4A). In the pachytene stage, SMNK-1::GFP fluorescence exhibited a punctate pattern that

gradually expanded. In the karyosome stage of prophase I, where FBs begins to assemble, the fluorescence of SMNK-1::GFP formed a boat-shaped pattern, which became enlarged in size during meiotic divisions (Fig. 4B). During the budding stage after anaphase II, most of SMNK-1::GFP fluorescent signals were partitioned into spermatids. When sperm were activated with Pronase, concentrated SMNK-1::GFP signal remained in the cell body, but not in the pseudopod of spermatozoon (Supplementary Fig.4B).

Given the facts that FBs are usually associated with MOs[9,11,23,23,25] and that loss of SMNK-1 specifically affects FBs formation in spermatocytes, causing MSP partitioning defects during budding stage and the failure of pseudopod extension during sperm activation, we hypothesize that the boat-shaped signal of SMNK-1::GFP fluorescence in spermatocytes is related to FB-MOs in the developing spermatocytes. To test this hypothesis, we conducted IFM assay. The MSP antibody-recognized FBs were surrounded by the GFP-labeled SMNK-1, displaying a partial colocalization pattern, especially at the edge of FBs (Fig. 4C). In spermatocytes, FBs are semi-enclosed by the membranes of ER/Golgi-derived MOs[3,25,26], therefore we checked the localization of SMNK-1::GFP relative to MOs, which could be recognized by its fiducial marker 1CB4[25,27–29]. We found that the presence of 1CB4-labeled MOs far preceded that of SMNK-1::GFP, and that SMNK-1::GFP colocalized with MOs once SMNK-1::GFP was visible (Supplementary Fig.4C).

SMNK-1 functions upstream of SPE-18

The expression pattern of SMNK-1 reminds of the SPE-18 protein, which, together with SPE-6, participates in MSP polymerization and FB formation[9,11]. SPE-18 localizes to developing spermatocytes to aid in MSP nucleation and assembly. We then aimed to determine if there is a relationship between the expression pattern of SPE-18 and SMNK-1. Using CRISPR-Cas9-based genome editing technology, we generated SPE-18::mCherry;*him-5* and *spe-18*

frameshift mutation strains. We found that the SMNK-1::GFP signal appeared earlier than the SPE-18::mCherry signal in pachytene stage (Fig. 5A) and that SMNK-1::GFP puncta and SPE-18::mCherry puncta partially co-localized in late pachytene stage (Figs. 5A and Supplementary Fig.5A). The SPE-18::mCherry hermaphrodites, however, showed a slight decrease in their fertility (Fig. 5C).

Given their spatially similar but temporally different localization patterns during meiosis, we speculated that SMNK-1::GFP might function upstream of SPE-18::mCherry during FB assembly. Loss of SMNK-1 or inactivation of SMNK-1 completely disrupted the SPE-18::mCherry puncta in spermatogenesis (Fig. 5D and Fig. 5E). Conversely, the *spe-18* mutation did not affect the punctate structure of SMNK-1::GFP in the prophase I of meiosis. (Supplementary Fig.5B). Combined with the study that SPE-18 is recruited to MOs[11], we conclude that MOs-localized SMNK-1 functions upstream of SPE-18, and it recruits SPE-18 to the surface of MOs to collaboratively initiate the packing of MSP filaments into FBs.

The MO acidification mediated by VHA-18 is required for FB-MO morphogenesis and SMNK-1 localization

During spermatogenesis, membraneless condensate FBs and membrane-bound MOs are closely interrelated. Each acidic MO (stained with LysoTracker Red)[24] was associated with the SMNK-1::GFP puncta in spermatocytes (Figs. 6A and 6B). The highly acidic pH of MOs' lumen implies that the alkalinization of the microenvironment outside of MOs might be required for FB assembly and/or FB-MO complex association. Vacuolar H^+ ATPases (v-ATPases) are ATP-dependent proton pumps that transport H^+ across membranes into vesicle lumens, utilizing energy from ATP hydrolysis[30,31]. The v-ATPase complex consists of the soluble V1 domain, which hydrolyzes ATP, and the membrane-embedded V0 domain, responsible for proton transport. v-ATPase activity supports intracellular substance transport and homeostasis.

To investigate the role of MOs played in MSP condensate assembly, we treated the sperm with Bafilomycin A1(BFA), which specifically binds to the c subunit of v-ATPase and inhibits its activity[32,33]. BFA treatment disrupted the MO acidification in spermatocytes and caused the punctate structure of SMNK-1::GFP to diffuse in the cytoplasm (Fig. 6C). Our genetic screen has identified a highly conserved H subunit of the v-ATPase, VHA-18 (Supplementary Fig.6A), required for spermatogenesis. Through CRISPR-Cas9-based genome editing, we generated an mCherry knock-in allele at *vha-18* loci. In the knock-in worms, VHA-18::mCherry was specifically expressed in male gonads and hermaphrodite spermatheca (Figs. S6B and S6C). VHA-18 was localized on the MOs probed by MO marker SAC-1 fused with GFP in spermatocytes[23] (Supplementary Fig.6D) and spermatids (Supplementary Fig.6E). Loss of VHA-18 resulted in some large and abnormal vacuoles scattered in the cell, unlike the scenario in the control, where MOs were docked underneath the PM via the membrane contact site formed between the head of MO and PM, as revealed by the fluorescence of LysoTracker Red (Figs. 6D, S6F and S6G) and by TEM (Supplementary Fig.7A). Meanwhile, the vesicular acidification was defective in *vha-18* spermatocytes and spermatids, as indicated by the diffusive fluorescence of LysoTracker Red in the cytoplasmic space among the vacuoles (Figs. 6D, S6F and S6G). Conversely, loss of SMNK-1, which affected FB assembly but without affecting MOs' structure and functions, did not alter the MO acidification (Figs. 2D and S6H). Additionally, we investigated the influence of *vha-18* mutation on SMNK-1::GFP and observed altered localization of SMNK-1::GFP in *vha-18* spermatocytes (Fig. 6D). These data suggest that MO-localized v-ATPase complex regulates the intracellular proton homeostasis by pumping the proton into the MO lumen, which might generate an alkaline cytoplasmic microenvironment around the MOs required for FB-MO complex morphogenesis.

VHA-18 is essential for spermatogenesis and fertility in *C. elegans*

We further investigated the influence of VHA-18 on spermatogenesis. We firstly compared the ultrastructure of spermatocytes using TEM. In the control group, FBs were semi-enclosed by the tubule-like MOs. In contrast, spermatocytes in *vha-18* mutant contained some FBs-associated vacuoles (Fig. 7A). Cryo-immuno EM analysis with 1CB4[11,25,28,34,35]or anti-serpin antibody[27] showed that these vacuoles were the defective MOs (Fig. 7B). In the late stage of spermatocytes of *vha-18* mutant, some FBs became naked and were no longer associated with vesicles, some other FBs were still associated with vesicles, but not semi-enclosed by the tubule-like MOs as seen in the control (Fig. 7A).

Disassociation of FBs with MOs in *spe-4* or *spe-10* spermatocytes affects MSP partitioning to spermatids during the budding division[25,34]. Building upon these findings, we hypothesized that *vha-18* mutant with disassociated FB and MOs might also affect MSP partitioning after anaphase II. Indeed, a significant amount of free MSP and FBs was detected in the RB of *vha-18* mutant using MSP antibody-based IFM (Fig. 7C). We also observed some other defects, including the presence of intact FBs and vacuoles revealed by TEM (Supplementary Fig.7A), incorrect GFP::NKB-2 localization (Supplementary Fig.7B), and multi-nuclei, in *vha-18* mutant spermatids.

Next, we checked the impact of *vha-18* on sperm activation. Most of spermatids containing several huge vacuoles from *vha-18* mutant failed to activate at all, and only a few partially activated sperm (indicated by the GFP puncta) with short pseudopod or only spiky projections in the same field could be observed (Fig. 7D). These results can be partially explained by the absence of the available MSP in the *vha-18* spermatids (Fig. 7C). Subsequently, we tested the fertility of *vha-18* mutant. The *vha-18* hermaphrodite produced less than half progeny of the wildtype (Fig. 7E). However, the reduced hermaphrodite fertility can be rescued by mating with *him-5* males (Fig. 7E), indicating a sperm defect in *vha-18* hermaphrodite. To test the male fertility, control (*him-8*) or *vha-18;him-8* males were mated with *spe-8;dpy-4* hermaphrodites, respectively. Most

progeny sired by *him-8* males appeared non-dumpy (cross progeny), while most of progeny sired by *vha-18;him-8* males were dumpy (hermaphrodite self-progeny) (Fig. 7F), indicating that *vha-18* male sperm are defective. Therefore, VHA-18 is required for the fertility in both hermaphrodites and males.

DISCUSSION

Cells need to carefully regulate the polymerization of their cytoskeletal components in terms of timing and location to ensure proper functioning. In nematode spermatocytes, it has been suggested that localized MSP polymerization is required for preparing MSP for post-meiotic division and preventing disruption of the meiotic divisions. In this study, we identified a sperm-specific casein-like kinase SMNK-1 required for spermatogenesis in *C. elegans* (Figs. 1A and 1B). The loss or the kinase activity-dead mutation of SMNK-1 results in the failure of FB assembly in spermatocytes (Fig. 3). The resultant spermatids contain no or less MSP, thus fail to activate, causing the sterility in both hermaphrodites and males (Fig. 1D and 1E). SMNK-1 is expressed primarily in the proximal arm of the male germline and exhibits a stage-specific pattern during spermatogenesis (Fig. 4B). In the pachytene stage, punctate SMNK-1 is localized on the surface of MOs and recruits SPE-18 to MOs. As spermatocytes progress to the diplotene stage, FBs composed of bundled MSP filaments gradually assemble, becoming semi-enveloped by the vesicular MO[36]. SMNK-1, together with SPE-18, localizes on the MO surface, displaying a pattern reminiscent of a boat, reflecting the topography of MO during MSP filaments sorting and FBs expansion (Fig. 5A). During the budding division that follows anaphase II, SMNK-1 predominantly partitions to the spermatids, appearing as faint dots in the sperm cytoplasm (Fig. 4B). Eventually, the head of MO will form stable membrane contact sites with PM, securing that the MOs will be sorted and partitioned into the developing spermatids, instead of RB, during budding. Therefore, we suggest that the interplay between membraneless condensate FBs and membrane-bound MOs is mutually beneficial to FBs and MOs.

In the nematode *C. elegans*, amoeboid sperm utilize the dynamics of cytoskeleton composed of MSP, in place of conventional actin, to power the cell motility and cell migration. Like that in mammals, each diploid spermatocyte in

C. elegans gives rise to four haploid spermatids. Each spermatid has only minimal organelles such as a central nucleus surrounded by some mitochondria and MOs, while the unnecessary cellular constituents for sperm maturation and sperm-oocyte recognition are disposed into an anucleate RB. In developing spermatocytes, several sperm-specific gene products are required to form the transient yet relatively solid FBs, which are composed of bundled MSP filaments and associated with the MOs. Once spermatid is budded off the RB, FBs will shortly dissemble into soluble MSP dimers. MSP constitutes about 25% of the total proteins present in sperm and accounts for about 80% of proteins in the pseudopod of spermatozoa. Thus, the interaction between membraneless condensate FBs and membrane-bound MO in spermatocyte might facilitate the correct sorting and transport of essential constituents during spermatogenesis.

SPE-18, an IDR-containing protein with several predicted phosphorylation sites in its C-terminal amino acid sequence, is required for FB formation and spermatogenesis[11]. SMNK-1 acts as an upstream protein kinase of SPE-18, and its kinase activity is essential for SPE-18's localization on the surface of MOs in spermatocytes. It has been confirmed that bacteria-expressed SPE-18 remains soluble at 95°C in vitro, demonstrating heat resistance. This suggests that SPE-18 may promote MSP condensate assembly via phase separation, with its activity potentially regulated by phosphorylation.[11]. Therefore, it is highly plausible that SMNK-1, together with SPE-18, may regulate the FB assembly through phase separation. Meanwhile, we also found that VHA-18, the H subunit of the v-ATPase, was localized on MOs in the spermatocytes, indicating that the v-ATPase may have been assembled in the spermatocytes and pump the nearby proton into the MOs' lumen, making the immediate cytoplasmic microenvironment around MOs more alkaline. This result is consistent with a previous study in which a higher pH is favorable for MSP polymerization in the leading edge of spermatozoa of *Ascaris suum*[37]. Loss of VHA-18 causes the defective FB-MO morphogenesis, and results in naked FBs in the cytoplasm of

vha-18 spermatocytes, thus affecting the efficiency and/or efficacy of MSP filaments sorting and partitioning to the spermatids.

MSP assembly into FBs in spermatocytes or meshwork cytoskeleton in the pseudopod of spermatozoa depends on the membrane either from MOs (this study) or PM[38–40], while MSP in dimer is soluble in mature spermatids. Thus, MSP are in three different phases: solid and less dynamic FBs, free and soluble dimers, and highly motile gel-like cytoskeleton. The membrane and its immediate microenvironment might define which phase MSP would be in. The cargo sorting mechanism via phase transition mediated by the interaction between membraneless condensate and membrane-bound organelles demonstrated in this study might apply to the intracellular macrobiomolecules (such as RNA), protein trafficking, or the fine-tuning of their activities from prokaryotic to eukaryotic cells. SMNK-1 functions upstream of SPE-18 and the kinase activity of SMNK-1 is necessary for recruiting SPE-18 to the surface of MOs. This is one of the key discoveries in this study. However, it remains unclear whether SMNK-1 and SPE-18 interact directly, or other unidentified proteins are involved. Moreover, SMNK-1 is a soluble protein without any transmembrane domain in its amino acid sequence. However, SMNK-1::GFP exhibits boat-like structure at the periphery of FBs, which are closely associated with MOs. Therefore, it is conceivable that SMNK-1 is recruited by unidentified protein or anchored to the MOs through some kinds of modifications. Further improvement of experimental techniques will help to clarify MSP dynamics mediated by SMNK-1 in *C. elegans* sperm.

REFERENCES

1. Agarwal, A., Baskaran, S., Parekh, N., Cho, C.-L., Henkel, R., Vij, S., Arafa, M., Panner Selvam, M.K., and Shah, R. (2021). Male infertility. The Lancet *397*, 319–333. https://doi.org/10.1016/S0140-6736(20)32667-2.

2. Gül, M., Russo, G.I., Kandil, H., Boitrelle, F., Saleh, R., Chung, E., Kavoussi, P., Mostafa, T., Shah, R., and Agarwal, A. (2024). Male Infertility: New Developments, Current Challenges, and Future Directions. World J Mens Health *42*, e8. https://doi.org/10.5534/wjmh.230232.

3. Miao, L., and L'Hernault, S.W. (2014). Role of Posttranslational Modifications in C. elegans and Ascaris Spermatogenesis and Sperm Function. In Posttranslational Protein Modifications in the Reproductive System Advances in Experimental Medicine and Biology., P. Sutovsky, ed. (Springer New York), pp. 215–239. https://doi.org/10.1007/978-1-4939-0817-2_10.

4. Hu, J., Cheng, S., Wang, H., Li, X., Liu, S., Wu, M., Liu, Y., and Wang, X. Distinct roles of two myosins in C. elegans spermatid differentiation.

5. Gleason, E.J., Hartley, P.D., Henderson, M., Hill-Harfe, K.L., Price, P.W., Weimer, R.M., Kroft, T.L., Zhu, G., Cordovado, S., and L'Hernault, S.W. (2012). Developmental Genetics of Secretory Vesicle Acidification During *Caenorhabditis elegans* Spermatogenesis. Genetics *191*, 477–491. https://doi.org/10.1534/genetics.112.139618.

6. Schreier, J., Dietz, S., Boermel, M., Oorschot, V., Seistrup, A.-S., De Jesus Domingues, A.M., Bronkhorst, A.W., Nguyen, D.A.H., Phillis, S., Gleason, E.J., et al. (2022). Membrane-associated cytoplasmic granules carrying the Argonaute protein WAGO-3 enable paternal epigenetic inheritance in Caenorhabditis elegans. Nat Cell Biol *24*, 217–229. https://doi.org/10.1038/s41556-021-00827-2.

7. Li, D., Huang, S., Chai, Y., Zhao, R., Gong, J., Zhang, Q.C., Ou, G., and Wen, W. (2023). A paternal protein facilitates sperm RNA delivery to regulate zygotic development. Sci China Life Sci. https://doi.org/10.1007/s11427-022-2332-5.

8. Smith, H. (2006). Sperm motility and MSP. WormBook. https://doi.org/10.1895/wormbook.1.68.1.

9. Varkey, J.P., Jansma, P.L., Minniti, A.N., and Ward, S. (1993). The Caenorhabditis elegans spe-6 gene is required for major sperm protein

assembly and shows second site non-complementation with an unlinked deficiency. Genetics *133*, 79–86. https://doi.org/10.1093/genetics/133.1.79.

10. Muhlrad, P.J., and Ward, S. (2002). Spermiogenesis Initiation in *Caenorhabditis elegans* Involves a Casein Kinase 1 Encoded by the *spe-6* Gene. Genetics *161*, 143–155. https://doi.org/10.1093/genetics/161.1.143.

11. Price, K.L., Presler, M., Uyehara, C.M., and Shakes, D.C. (2021). The intrinsically disordered protein SPE-18 promotes localized assembly of MSP in *Caenorhabditis elegans* spermatocytes. Development *148*, dev195875. https://doi.org/10.1242/dev.195875.

12. Ma, X., Zhu, Y., Li, C., Xue, P., Zhao, Y., Chen, S., Yang, F., and Miao, L. (2014). Characterisation of Caenorhabditis eleganssperm transcriptome and proteome. BMC Genomics *15*, 168. https://doi.org/10.1186/1471-2164-15-168.

13. Ebbing, A., Vértesy, Á., Betist, M.C., Spanjaard, B., Junker, J.P., Berezikov, E., Van Oudenaarden, A., and Korswagen, H.C. (2018). Spatial Transcriptomics of C. elegans Males and Hermaphrodites Identifies Sex-Specific Differences in Gene Expression Patterns. Developmental Cell *47*, 801-813.e6. https://doi.org/10.1016/j.devcel.2018.10.016.

14. Reinke, V., Gil, I.S., Ward, S., and Kazmer, K. (2004). Genome-wide germline-enriched and sex-biased expression profiles in Caenorhabditis elegans. Development *131*, 311–323. https://doi.org/10.1242/dev.00914.

15. Peterson, J.J., Tocheny, C.E., Prajapati, G., LaMunyon, C.W., and Shakes, D.C. (2021). Subcellular patterns of SPE-6 localization reveal unexpected complexities in *Caenorhabditis elegans* sperm activation and sperm function. G3 Genes|Genomes|Genetics *11*, jkab288. https://doi.org/10.1093/g3journal/jkab288.

16. Manning, G. (2005). Genomic overview of protein kinases. WormBook. https://doi.org/10.1895/wormbook.1.60.1.

17. Muhlrad, P.J., Clark, J.N., Nasri, U., Sullivan, N.G., and LaMunyon, C.W. (2014). SPE-8, a protein-tyrosine kinase, localizes to the spermatid cell membrane through interaction with other members of the SPE-8 group spermatid activation signaling pathway in C. elegans. BMC Genet *15*, 83. https://doi.org/10.1186/1471-2156-15-83.

18. Smith, J.R., and Stanfield, G.M. (2011). TRY-5 Is a Sperm-Activating Protease in Caenorhabditis elegans Seminal Fluid. PLoS Genet *7*, e1002375. https://doi.org/10.1371/journal.pgen.1002375.

19. Stanfield, G.M., and Villeneuve, A.M. (2006). Regulation of Sperm

549 Activation by SWM-1 Is Required for Reproductive Success of C. elegans
550 Males. Current Biology *16*, 252–263.
551 https://doi.org/10.1016/j.cub.2005.12.041.

552 20. Singson, A., Hill, K.L., and L'Hernault, S.W. (1999). Sperm Competition in
553 the Absence of Fertilization in Caenorhabditis elegans. Genetics *152*, 201–
554 208. https://doi.org/10.1093/genetics/152.1.201.

555 21. LaMunyon, C.W., and Ward, S. (1995). Sperm predence in a hermaphroditic
556 nematode (Caenorhabditis elegans) is due to competitive superiority of
557 male sperm. Experientia *51*, 817–823. https://doi.org/10.1007/BF01922436.

558 22. Hansen, J.M., Chavez, D.R., and Stanfield, G.M. (2015). COMP-1 promotes
559 competitive advantage of nematode sperm. eLife *4*, e05423.
560 https://doi.org/10.7554/eLife.05423.

561 23. Wang, Q., Cao, Z., Du, B., Zhang, Q., Chen, L., Wang, X., Yuan, Z., Wang,
562 P., He, R., Shan, J., et al. (2021). Membrane contact site-dependent
563 cholesterol transport regulates Na+/K+-ATPase polarization and
564 spermiogenesis in Caenorhabditis elegans. Developmental Cell *56*, 1631-
565 1645.e7. https://doi.org/10.1016/j.devcel.2021.05.002.

566 24. Machaca, K., and L'Hernault, S.W. (1997). The *Caenorhabditis elegans*
567 *spe-5* Gene Is Required for Morphogenesis of a Sperm-Specific Organelle
568 and Is Associated With an Inherent Cold-Sensitive Phenotype. Genetics
569 *146*, 567–581. https://doi.org/10.1093/genetics/146.2.567.

570 25. Arduengo, P.M., Appleberry, O.K., Chuang, P., and L'Hernault, S.W. (1998).
571 The presenilin protein family member SPE-4 localizes to an ER/Golgi
572 derived organelle and is required for proper cytoplasmic partitioning during
573 *Caenorhabditis elegans* spermatogenesis. Journal of Cell Science *111*,
574 3645–3654. https://doi.org/10.1242/jcs.111.24.3645.

575 26. Clark, J.N., Prajapati, G., Aldaco, F.K., Sokolich, T.J., Keung, S.S., Austin,
576 S.P., Valdés, Á.A., and LaMunyon, C.W. (2020). Functionally non-redundant
577 paralogs spe-47 and spe-50 encode FB-MO associated proteins and
578 interact with him-8. PLoS ONE *15*, e0230939.
579 https://doi.org/10.1371/journal.pone.0230939.

580 27. Zhao, Y., Sun, W., Zhang, P., Chi, H., Zhang, M.-J., Song, C.-Q., Ma, X.,
581 Shang, Y., Wang, B., Hu, Y., et al. (2012). Nematode sperm maturation
582 triggered by protease involves sperm-secreted serine protease inhibitor
583 (Serpin). Proc. Natl. Acad. Sci. U.S.A. *109*, 1542–1547.
584 https://doi.org/10.1073/pnas.1109912109.

585 28. Nichol, J. (1985). Monoclonal Antibodies Which Distinguish Certain Classes

of Neuronal and Supporting Cells in the Nervous Tissue of the Nematode Caenorhabdifis Elegans'. The Journal of Neuroscience *5*.

29. Washington, N.L., and Ward, S. (2006). FER-1 regulates Ca2+-mediated membrane fusion during *C. elegans* spermatogenesis. Journal of Cell Science *119*, 2552–2562. https://doi.org/10.1242/jcs.02980.

30. Futai, M., Sun-Wada, G.-H., Wada, Y., Matsumoto, N., and Nakanishi-Matsui, M. (2019). Vacuolar-type ATPase: A proton pump to lysosomal trafficking. Proc. Jpn. Acad., Ser. B *95*, 261–277. https://doi.org/10.2183/pjab.95.018.

31. Lee, S.-K., Li, W., Ryu, S.-E., Rhim, T., and Ahnn, J. (2010). Vacuolar (H+)-ATPases in Caenorhabditis elegans: What can we learn about giant H+ pumps from tiny worms? Biochimica et Biophysica Acta (BBA) - Bioenergetics *1797*, 1687–1695. https://doi.org/10.1016/j.bbabio.2010.07.004.

32. Wang, R., Wang, J., Hassan, A., Lee, C.-H., Xie, X.-S., and Li, X. (2021). Molecular basis of V-ATPase inhibition by bafilomycin A1. Nat Commun *12*, 1782. https://doi.org/10.1038/s41467-021-22111-5.

33. Bowman, B.J., and Bowman, E.J. (2002). Mutations in subunit C of the vacuolar ATPase confer resistance to bafilomycin and identify a conserved antibiotic binding site. J Biol Chem *277*, 3965–3972. https://doi.org/10.1074/jbc.M109756200.

34. Gleason, E.J., Lindsey, W.C., Kroft, T.L., Singson, A.W., and L'Hernault, S.W. (2006). *spe-10* Encodes a DHHC–CRD Zinc-Finger Membrane Protein Required for Endoplasmic Reticulum/Golgi Membrane Morphogenesis During *Caenorhabditis elegans* Spermatogenesis. Genetics *172*, 145–158. https://doi.org/10.1534/genetics.105.047340.

35. Wu, J., Go, A.C., Samson, M., Cintra, T., Mirsoian, S., Wu, T.F., Jow, M.M., Routman, E.J., and Chu, D.S. (2012). Sperm Development and Motility are Regulated by PP1 Phosphatases in *Caenorhabditis elegans*. Genetics *190*, 143–157. https://doi.org/10.1534/genetics.111.135376.

36. Kosinski, M., McDonald, K., Schwartz, J., Yamamoto, I., and Greenstein, D. (2005). *C. elegans* sperm bud vesicles to deliver a meiotic maturation signal to distant oocytes. Development *132*, 3357–3369. https://doi.org/10.1242/dev.01916.

37. King, K.L., Essig, J., Roberts, T.M., and Moerland, T.S. (1994). Regulation of the *Ascaris* major sperm protein (MSP) cytoskeleton by intracellular pH. Cell Motil. Cytoskeleton *27*, 193–205.

https://doi.org/10.1002/cm.970270302.

38. Miao, L., Vanderlinde, O., Stewart, M., and Roberts, T.M. (2003). Retraction in Amoeboid Cell Motility Powered by Cytoskeletal Dynamics. *302*.

39. Miao, L., Vanderlinde, O., Liu, J., Grant, R.P., Wouterse, A., Shimabukuro, K., Philipse, A., Stewart, M., and Roberts, T.M. (2008). The role of filament-packing dynamics in powering amoeboid cell motility. Proc Natl Acad Sci.

40. Italiano, J.E., Roberts, T.M., Stewart, M., and Fontana, C.A. (1996). Reconstitution In Vitro of the Motile Apparatus from the Amoeboid Sperm of Ascaris Shows That Filament Assembly and Bundling Move Membranes. Cell *84*, 105–114. https://doi.org/10.1016/S0092-8674(00)80997-6.

41. Brenner, S. (1974). The Genetics of Caenorhabditis elegans. Genetics *77*, 71–94. https://doi.org/10.1093/genetics/77.1.71.

METHODS DETAILS

C. elegans strains and culture

Most *C. elegans* strains were maintained at 20℃ and cultured on plates containing nematode growth medium seeded with OP50 *E. coli* as the food source, as previously reported[41]. Besides, several strains used in this study were cultured at 16℃ and then shifted to 25℃ during the egg stage to induce temperature-sensitive phenotypes, such as *fem-1(hc17), fem-3(q96)*, and *glp-4(bn2)*. *him-5(e1490) or him-8 (e1489)* was used as the control in most experiments to ensure an adequate number of males for the assays. Knock-out strains *smnk-1(ibp107), smnk-1(ibp116), smnk-1(ibp129),* and *spe-18(ibp158),* as well as knock-in strains SMNK-1::GFP, SPE-18::mCherry, and SPE-6::mCherry, were generated using the CRISPR-Cas9 genome editing system. Other strains were provided by the Caenorhabditis Genetics Center or from our laboratory collection.

Molecular biology techniques for transgenic strain construction

The CRISPR-Cas9-based genome editing was performed using the plasmid pDD162 carrying the target gene sequence. The target sequence for knock-out was obtained from the online CRISPR design website (https://sg.idtdna.com/site/order/designtool/). Prior to inserting the target sequence into the pDD162 plasmid, the plasmid was PCR-amplified using Q5 high-fidelity DNA polymerase (New England Biolabs) with the primers listed in Table 1. Subsequently, the PCR products were digested with DpnI (New England Biolabs) for 2 h at 37℃ and transformed into DH5α competent cells.

For the construction of the *smnk-1::gfp, spe-6::mCherry, spe-18::mCherry,* and *vha-18::mCherry* template plasmids for homologous recombination, the pPD95.75 plasmid served as the backbone and donor of the *gfp* sequence. Additionally, the pCFJ150-mCherrydPiRNA plasmid (a gift from Dr. Donglei Zhang Lab from Huazhong University of Science and Technology) was utilized as the donor of the *mCherry* sequence. The sgRNA target sequences were selected in close proximity to the stop codon of *smnk-1, spe-6, spe-18* or *vha-18* sequence. An approximately 2 kb fragment, encompassing segments of approximately 1 kb flanking the 5' and 3' ends of the target sequence in the genome, was ligated into the *gfp*-removed fragment from pPD95.75. The 2 kb fragment was PCR-amplified using the N2 or *him-5* worm lysate as the template. The ligation was carried out using the ClonExpress II One Step Cloning Kit (Vazyme). Subsequently, the *gfp* or *mCherry* fragment without a stop codon was PCR-amplified and ligated into the plasmid containing the 2 kb fragment immediately before the stop codon of *smnk-1*, *spe-6*, *spe-18 or vha-18.* A linker region (5'-AGCTTGCATGCCTGCAGGTCGACTCTAGAGGATCCCCGGGATTGGCCAAAGGACCCAAAGGTATGTTTCGAATGATACTAACATAACATAGAACATTTTCAGGAGGACCCTTGGAGGGTACCGGTAGAAAAA-3') was inserted at the 5' end of the *gfp* or *mCherry* sequences of *smnk-1, spe-6*, *spe-18 or vha-18*. Synonymous coding sequences were introduced into the sgRNA targeting

sequence in the plasmid via PCR to prevent Cas9 cleavage activity. The constructed template plasmid, pDD162, contains the target sequence. pDD162 and the pRF4 plasmid, which carries the dominant Roller marker *rol-6(su1006)*, were microinjected into young adult N2 hermaphrodites at a concentration of 70 ng/mL.

To generate the point mutation which might lead to the inactivation of SMNK-1, we substituted the putative site T195 in the activation loop of SMNK-1 with A. Like the process described above, a 2 kb fragment containing approximately 1 kb upstream and 1 kb downstream of the T195 locus was amplified by PCR and then ligated into the *gfp*-removed fragment from pPD95.75. Subsequently, the T195A point mutation and synonymous coding sequences were introduced into the plasmid through PCR. This template was co-injected with pRF4 and pDD162 that carries the target sequence.

Fertility assays

To determine hermaphrodite fertility, we placed a single L4 stage hermaphrodite with ~ 20 replicates on each plate. The hermaphrodite was then transferred to a new marked plate every day until no egg was laid, and the number of progeny sired by each hermaphrodite was counted after they grew up.

For the hermaphrodite fertility rescue assay, one L4 hermaphrodite and three virgin adult males were placed on a mating plate with an *E. coli* bacterial lawn and cultured for 24 h, thus the males would have enough time to mate with the hermaphrodites and transfer sperm to the hermaphrodite uterus. Subsequently, the males were removed, and the hermaphrodites were transferred to individual fresh plates every day until no progeny was sired. The number of progeny sired by each hermaphrodite was counted.

To assess male fertility potential, we placed three one-day post-L4 virgin males and one L4 *spe-8;dpy-4* hermaphrodite to a mating plate for 24 h. The males

were removed afterward, and the hermaphrodite was transferred to an individual plate every day until no progeny was sired. The number of normal or dumpy phenotype progeny sired by each hermaphrodite was counted.

Sperm activation assays

L4 males were selected and cultured for 48-60 h to accumulate sufficient sperm. Subsequently, the males were dissected in a 3.5 μL Sperm Medium (SM buffer: 50 mM HEPES, 50 mM NaCl, 25 mM KCl, 1 mM $MgSO_4$, 5 mM $CaCl_2$, and 10 mg/mL polyvinylpyrrolidone, pH 7.8) and perfused with various activators (200 mg/mL Pronase, 1 mM $ZnSO_4$, 40 mM NH_4Cl, 30 mM TEA, or 40 nM monensin) along with membrane dyes (10 mg/mL FM 1-43; Invitrogen) prepared in SM buffer. Images were captured using the FV1200 confocal microscope.

Motility assay of male spermlabeled by MitoTracker Red

To assess the male-derived sperm motility after sperm activation in vivo, we cultured two-day post-L4 virgin males overnight in mating plate containing 50 μM MitoTracker Red. Labeled males and L4 wildtype hermaphrodite (ration 3:1) were then placed on normal mating plate for 8 h. Subsequently, the hermaphrodites were isolated and transferred to new plates for an additional 30 min. The hermaphrodites were then placed on a 2% agarose pad and anesthetized with 0.1 mM levamisole in M9 buffer. The position of male sperm in hermaphrodite was observed by MitoTracker fluorescence with FV3000 confocal microscopy.

Transmission electron microscopy

Caenorhabditis elegans males at 48 h post-L4 stage were placed into 4 μL of SM buffer on poly-lysine-coated Thermanox plastic coverslip and cut to release

sperm or gonad. The sperm or gonad was fixed by adding 100 μL SM buffer containing 2.5% glutaraldehyde for 2 h. The samples were post-fixed with 1% osmium tetroxide for 2 h on ice, stained with 1% uranyl acetate overnight at 4℃, and dehydrated with a graded series of ethanol followed by acetone transition. Then, the samples were embedded in a flat mold with fresh Embed 812 resin and polymerized in an oven at 60℃ for 48 h. The coverslips were then peeled off, leaving the sample on the surface of the resin block. The trimmed block with sample facing out was glued to a supporting blank resin block. Ultrathin sections (~80 nm) were cut on Leica EM UC7 ultramicrotome (Leica, Germany) and observed on an FEI Tecnai Spirit 120 electron microscope at 100 kV.

Immunofluorescence microscopy assay

Spermatids or spermatocytes dissected from virgin males at 30-48 h after the L4 stage were fixed with 4% paraformaldehyde in SM buffer overnight at 4℃. After being washed three times with PBS, the sperm were permeabilized with 1% Triton X-100 for 30 min and blocked with 2% BSA in PBS for 4-6 h. Subsequently, the sperm were incubated with diluted primary antibodies (MSP 1:50 or GFP 1:200) at 4℃ overnight. The sperm were washed for three times with PBS and then incubated with diluted Alexa 488-conjugated goat anti-mouse antibody (1:400; Invitrogen) or Alexa 546-conjugated goat anti-rabbit antibody (1:400; Invitrogen) at room temperature for 2 h. Following another three times of washing with PBS, the slides were sealed and analyzed using the FV3000 confocal microscope.

For the germline Immunofluorescence microscopy assay, male germlines were dissected in SM buffer on a poly-lysine pad, then fixed and permeabilized with pre-cooled methanol at -20℃ overnight. After washing three times with PBS, the germlines were blocked with 0.5% BSA and 0.1% tween-20 in M9 for 30 min and incubated with diluted primary antibody for 2h at room temperature.

The subsequent steps were the same as those for sperm immunofluorescence.

Cryo immunoelectron microscopy

Caenorhabditis elegans at 48 h post-L4 stage were transferred to an SM buffer on a Thermanox plastic coverslip, and dissected to release sperm or gonad. The sample was fixed with 100 μL cool PB buffer containing 4% paraformaldehyde and 0.1% glutaraldehyde at 4℃ for 2 h. Processing of samples for ultrathin cryosectioning and immunolabeling according to the protein A-gold method was done as described previously (Sachse et al., 2002). In brief, fixed samples were embedded in 12% gelatin in 0.1 M PB at 37℃. After solidification on ice, the gelatin block was cut into small blocks. The small blocks were infiltrated with 2.3 M sucrose at 4℃ for two days, and then mounted on cryospecimen pins, and then frozen in liquid nitrogen. Ultrathin cryosections (80 nm thickness) were cut with an ultramicrotome (Leica EM FC7) and transferred to formvar-coated grids through a mixture of 2.3 M sucrose and 2% methylcellulose. Ultrathin cryosections were immunogold-labeled and stained as described before (Sachse et al., 2002). In brief, the thawed sections were blocked with 100 mM glycine for 5 min and then incubated for 2 h with the primary antibody (rabbit anti-serpin polyclonal antibody, 1:400 or mouse 1CB4 monoclonal antibody, 1:100) and subsequently with gold-conjugated secondary antibody (15 nM goat anti-rabbit antibody or 10 nM goat anti-mouse antibody, respectively. 1:100) for 1 h. In the negative group, incubation with the primary antibody was omitted. Samples were floating for fixation on a droplet of 2.5% glutaraldehyde in PBS for 5 min, and collected with a wire loop with adhering droplet of 0.2% uranyl acetate and 1.8% methylcellulose. The cryosections were observed and photographed in a Tecnai Spirit 120 kV transmission electron microscope (FEI) at 100 kV.

Resource availability

Further information and requests for resources and reagents should be directed to and will be fulfilled by the Lead Contact, Long Miao (lmiao@bnu.ac.cn).

Materials availability

All unique/stable materials generated in this study are available from the Lead Contact upon request.

Data and code availability

This study did not generate unique code or dataset.

Acknowledgments

We are grateful to Dr. Fanxia Meng for her helpful comments and manuscript editing. We thank Dr. Steven W. L'Hernault for providing antibody, Dr.s Guangshuo Ou and Donglei Zhang for providing plasmids. We thank the staff members at the Center for Biological Imaging, the Institute of Biophysics, Chinese Academy of Sciences, for their support in image collection. This work was supported by grants from the National Key Research and Development Program of China (2023YFA1801100 to L.M.), the Natural Science Foundation of China (32070694 to Y.Z., 32270774 to L.M.). Y.L. is supported by the funding from Applied Biological/Medical Disciplines Construction of Anhui Province. Some strains were obtained from the *Caenorhabditis* Genetics Center, which is funded by the National Institutes of Health Office of Research Infrastructure Programs (P40 OD010440).

Author contributions

X.M., X.C., P.W., Y. Z., and L.M. designed the experiments; Most molecular and cell biology experiments were performed by X.M., X.C. and P.W., L.C. conducted the TEM and Cryo-immuno EM study. X.M., X.C., L.C., P.W., Y.Z. and L.M. analyzed the data and wrote the manuscript with input from all authors.

Declaration of interests

The authors declare no competing interests.

Figure legends

Fig. 1. Casein-like kinase SMNK-1 is required for *C. elegans* fertility.

(A) RT-PCR showed the relative expression of *smnk-1* in N2 and *fem-1 (hc17), fem-3(q96 gf)* and *glp-4(bn2)* mutants, with *act-1* serving as the control. *fem-1 (hc17) and fem-3* (q96 gf) worms only produced oocytes and sperm, respectively, while *glp-4(bn2)* worms displayed defective germline development and do not produce either oocytes or sperm.

(B) Quantification of relative *smnk-1* expression shown in (A). values are means ± SEM. ****, P<0.0001. NS, not significant.

(C) Genomic structure of *smnk-1* gene. The boxes represent exons, and the solid lines represent introns. The mutations are labeled at their corresponding positions. *smnk-1 (ibp107)* is a frameshift mutation caused by a 7 bp insertion in the first exon. *smnk-1(ibp129)* is a point mutation at the putative active site residue T195; *smnk-1(ibp116)* is terminated at the 294th amino acid, thus a C-terminus deletion mutant. *smnk-1(ibp129)* and *smnk-1(ibp116)* are two alleles that might affect kinase activity of SMNK-1.

(D) The *smnk-1* mutant hermaphrodites sired fewer progeny compared with control group, and the loss of fertility in *smnk-1* hermaphrodite could be rescued by mating with *him-5* males.

(E) *smnk-1* mutant males had impaired fertility. The number of cross progeny (ND, non-Dumpy) and self (D, Dumpy) progeny produced by *spe-8;dpy-4* hermaphrodites was counted after mating with control *him-5* or *smnk-1; him-5* males. Values in (D) and (E) are presented as the mean ± SEM. ****p < 0.0001, in comparison to the control.

(F) Sperm ejaculated from *smnk-1(ibp107)* males failed to migrate toward and accumulate in the spermatheca, unlike the behavior of sperm from control males. Males were stained with MitoTracker Red before mating with L4 virgin hermaphrodites. The arrow showed the MitoTracker Red-labeled male sperm from *smnk-1;him-5* males located outside of the hermaphrodite uterus, which might be pushed out of the uterus during egg-laying. Scale: 50 μm.

Fig. 2: *smnk-1* affects sperm activation and motility.

(A) Loss of *smnk-1* slightly affected hermaphrodite sperm activation, whichwas reflected by the number of GFP puncta on spermatozoa located in the spermatheca. Scale bars in left and right panels represent 20 and 10 μm, respectively.

(B) The dissected sperm from male gonad of *smnk-1;swm-1;gfp::nkb-2;him-5* and control group. In vivo activated *smnk-1* sperm nearly had no pseudopod, though GFP::NKB-2 displaying a polarized pattern. Scale: 5 μm.

(C) *smnk-1* affected sperm activation in vitro with extracellular sperm activators. SM represented the sperm medium, serving as the inactivated control; the known sperm activators, such as weak bases (NH_4Cl and TEA), the proton carrier monensin, trace element Zn^{2+}, and Pronase, were used to trigger sperm activation. The MO fusions were indicated by the fluorescent puncta of membrane impermeable probe FM 1-43. Scale: 5 μm.

(D) *smnk-1* spermatids contained normal MOs as seen in control. The acidic MOs were labeled with LysoTracker Red. Scale: 5 μm.

(E) Quantification of the number of the MOs indicated by LysoTracker Red shown in (D).

(F) *smnk-1* affected MO fusion and pseudopod extension when sperm were activated by Pronase. The fluorescent puncta of GFP::NKB-2 was used to indicate the fused MOs. Scale: 5 μm.

(G) Quantification of the number of fused MOs indicated by GFP::NKB-2 puncta fluorescence in (F). Values in (E) and (G) are presented as the mean ± SEM. ****$p < 0.0001$. NS, not significant.

Fig. 3. *smnk-1* affects FB assembly in spermatocytes.

(A) The anti-MSP immunofluorescence microscopy assay of spermatids from *smnk-1(ibp107)* and control males. Scale: 5 μm.

(B) Quantification of MSP fluorescence shown in (A). Values are presented as the mean ± SEM. ****p < 0.0001.

(C) The anti-MSP immunofluorescence microscopy assay of spermatocytes from *smnk-1(ibp107)* and control males in different stages. Green puncta observed in control cells indicate FBs. MSP fluorescence appeared diffusive in the cortical area of *smnk-1(ibp107)* spermatocytes in anaphase I stage and in the cortex of RB during budding stage Scale: 5 μm.

(D) The anti-MSP immunofluorescence microscopy assay of male gonads of *smnk-1(ibp116), smnk-1(ibp129)*, and control wroms. MSP immunofluorescence appeared diffusive in *smnk-1(ibp116)* and *smnk-1(ibp129)* gonad, unlike the fluorescent puncta (FBs) observed in the control. Scale: 10 μm.

(E) Quantification of MSP fluorescence shown in (D). Values are presented as the mean ± SEM. ****p < 0.0001.

(F) EM images of spermatocytes from *smnk-1(ibp107)* and control males. White arrows: tubule-like MOs; red arrows in the left panels: FBs semi-enclosed by MOs; m: mitochondria. Scale: 500 nm.

(G) EM images of sperm and RB in the budding stage from *smnk-1(ibp107)* and control males. Red arrows: FB-MO complex in control spermatids; The white dashed ellipse on the right showed the MO components, typically partitioned to spermatids, were lagged in RB in *smnk-1;him-5*. m: mitochondrion; N: nucleus. Scale: 1 μm.

Fig. 4. Punctate SMNK-1 is associated with FBs in spermatocytes.

(A) The shape and size of the nuclei labeled by Hoechst illustrated the various developmental stages in the male gonad. Scale bars in the left and right panels represent 50 μm and 20 μm, respectively.

(B) The expression and localization pattern of SMNK-1::GFP in the male gonad. The arrow indicated the boat-like structure of GFP puncta. The nuclei were labeled by Hoechst. Scale bars in the upper and lower panels represent 10 μm.

(C) Immunofluorescence microscopy assay showed that SMNK-1(green) was localized to the periphery of FBs (red) in meiotically dividing spermatocytes. The nuclei were labeled by DAPI. Scale: 10 μm.

(D) Quantification of MSP and SMNK-1::GFP fluorescence in the dashed line shown in (C).

Fig. 5. SMNK-1 functions upstream of SPE-18 and is required for recruiting SPE-18 to MOs.

(A) Live-cell imaging of SMNK-1::GFP and SPE-18::mCherry in different stages of spermatogenesis indicated by the nuclear size and structure. The appearance of SMNK-1::GFP occurred earlier than SPE-18::mCherry in the male gonad. The boxed areas in the upper panelwere magnified on the lower panels. Scale bars in the upper and lower panels represent 10 and 5 μm, respectively.

(B) Quantification of SPE-18::mCherry and SMNK-1::GFP fluorescence intensity along the dashed line shown in (A).The upper and lower images correspond to the dashed lines in magnified b and c, respectively.

(C) Inserting mCherry into the C-terminal of SPE-18 affected the fertility of hermaphrodites. values are presented as the mean ± SEM. ****$p < 0.0001$.

(D) Loss of SMNK-1 affected the localization of SPE-18::mCherry during spermatogenesis. In the control, SPE-18::mCherry appeared as puncta, while in any of the three *smnk-1* mutants, SPE-18::mCherry appeared diffusive in the cytoplasm. The boxed areas in the left are magnified on the right. Scale bars in left and right panels represent 20 and 10 μm, respectively.

(E) Quantification of SPE-18::mCherry fluorescence intensity in the dashed lines shown in (D).

Fig. 6. The acidification of MO lumen mediated by v-ATPase is required for FB-MO morphogenesis.

(A) SMNK-1::GFP puncta were localized on the surface of acidic MOs probed by the LysoTracker Red. Scale: 5 μm.

(B) Quantification of the SMNK-1::GFP fluorescence intensity in the dashed line shown in (A).

(C) BFA treatment neutralized the lumen of MOs and caused the puncta of SMNK-1::GFP to diffuse in spermatocytes. Scale: 20 μm.

(D) Loss of VHA-18 caused abnormal vacuoles scattered in the cytoplasm and the failure of SMNK-1::GFP condensation in spermatocytes. Many big round and scattered vacuoles were not stained by LysoTracker Red in *vha-18* spermatocyte. Meanwhile, the cytoplasmic space among vacuoles was stained heavily by LysoTracker Red, instead of the MOs lumen observed in the control. The fluorescence of SMNK-1::GFP appeared as puncta in the distal end, but decreased dramatically and failed to colocalize with LysoTracker Red in the area of spermatocyte in the proximal germline of *vha-18* male. The white boxes indicate the spermatocytes undergoing meiotic divisions. Scale: 5 μm.

Fig. 7. VHA-18 is required for MO-FB complex morphogenesis and male fertility.

(A) EM images of spermatocytes in dissected male gonad from *vha-18;him-8* or *him-8* control. Many vesicles were observed in *vha-18;him-8* spermatocytes. At the early stage of spermatocytes in *vha-18;him-8* (Panel c), some assembled FBs were associated with the abnormal vesicles, unlike that seen in control where tubule-like MOs semi-enclose the FBs (Panels a and b); at the late stage of spermatocytes in *vha-18;him-8* (Panel d), FBs expanded in both length and width were naked and not associated with the vacuoles. FB and MO membranes are labeled with white and yellow arrow, respectively. Scale: 500 nm.

(B) Cryo-immuno EM analysis of *vha-18;him-8* and *him-8* control spermatocytes. Both MO membrane and vacuole membrane were recognized by 1CB4 (Panels a and b) and serpin antibody (Panel d). A smaller MO head (Panel b, the white dashed circle), and a swollen MO body (Panels b, c and d) could be observed in *vha-18;him-8* spermatocytes, unlike that seen in control spermatocytes where normal sized MO head was connected via neck region to well-organized interrelated MO body (Panel a). The boxed areas in the upper panel were magnified on the lower panels. The antibody-conjugated colloidal gold particle can be distinctly observed in the bottom magnified panels a, b and d, but not panel c, which is the control without the primary antibody included. m: mitochondria; N: nucleus. The scale bar upper, 400 nm; the lower, 200 nm

(C) VHA-18 was necessary for MSP sorting after anaphase II. Immunofluorescence microscopy assay with MSP antibody showed that though some big MSP puncta could be observed in the budding spermatids, dramatic amount of MSP was retained in the RB in *vha-18;him-8*. MSP puncta appeared relatively similar in size and number in the budding spermatids and barely visible in RBs in the control. The white arrow and arrowhead indicated the dividing spermatids and RB, respectively. Scale: 5 μm.

(D) Loss of VHA-18 causeed sperm activation defects. TEA was used as extracellular agent to activate sperm. In the *vha-18* mutant sperm, a diminished presence of fused MOs (as indicated by reduced GFP::NKB-2

puncta) and shorter pseudopods or spiky projections were observed in comparison to the control group. Scale: 5 μm.

(E) Loss of VHA-18 affected hermaphrodite fertility. The reduced fertility of *vha-18* mutant hermaphrodites was rescued by mating with *him-5* males.

(F) Loss of VHA-18 affected male fertility. The number of cross progeny (ND, non-dumpy) or self-progeny (D, dumpy) produced by *spe-8;dpy-4* hermaphrodites are counted after mating with *him-8* or *vha-18;him-8* mutant males.

Supplementary Figure Legends

Fig. S1. SMNK-1 is a casein-like kinase required for spermatogenesis.

(A) Sequence alignment of the amino acids in SMNK-1 and other CK1 kinases. "*"represents identical amino acids. ":" represents amino acids with high similarity. "." represents amino acids with less similarity. Top to bottom: *Caenorhabditis brenneri* protein CBN18218, *Caenorhabditis elegans* protein SMNK-1, *Caenorhabditis remanei* protein CRE07959, *Caenorhabditis elegans* protein SPE-6 and human CK1ε. The sequence starting from DFG amino acids marked with a red line is the putative activation loop in the kinase domain. The T labeled by red triangle is the conserved amino acid that is necessary for kinase activity in CK1 family.

(B) The amino acid information of *smnk-1* alleles. *smnk-1(ibp107)* is a frameshift mutation caused by a 7 bp insertion in the first exon, resulting in a premature termination at the 71th amino acid. *smnk-1(ibp129)* is a point mutation (T195A) at the conserved active site; *smnk-1(ibp116)* is a C-terminus deletion allele.

(C) The number of oocytes laid by *smnk-1(ibp107);him-5 and him-5* control.

(D) The fertility of *smnk-1 (ibp107)* hermaphrodites was not temperature-sensitive. There was no significant difference in hermaphrodite fertility of *smnk-1(ibp107)* at 15 ℃, 20 ℃ and 25 ℃. Values in (C) and (D) are presented as the mean ± SEM. ****p < 0.0001.

Fig. S2. *smnk-1* does not affect spermatogenesis.

(A) Loss of SMNK-1 did not affect hermaphrodite spermatogenesis. The live-cell image was captured before the first ovulation of L4 stage. GFP::NKB-2 was localized uniformly on the PM of spermatocytes and spermatids with their nucleus highlighted by H2B::mCherry fluorescence. Scale: 20 μm.

Fig. S3. Loss of SMNK-1 does not affect MSP mRNAs level when compared with the control.

(A) RNA-seq analysis showed that all identified MSP mRNAs level did not change significantly in *smnk-1* compared to that in control, as revealed by the value of $\log_2$fc(*him-5/smnk-1*).

Fig. S4. SMNK-1 is mainly expressed in the gonad during spermatogenesis.

(A) The distribution of SMNK-1::GFP in hermaphrodites and males. The autofluorescence in *him-5* males and hermaphrodites were shown in the left panels. Scale: 200 μm.

(B) Live-cell imaging of SMNK-1::GFP in dividing spermatocytes and sperm. Scale: 5 μm.

(C) The immunofluorescence microscopy analysis showed the localization of 1CB4 (Red, MO marker) and SMNK-1::GFP puncta in the male gonad. The box 1 (more distal) indicated the area where 1CB4 labeling was visible but SMNK-1::GFP fluorescence was absent. The box 2 (more proximal) indicated the area where SMNK-1::GFP puncta (green) were partially colocalized with MOs (red). Scale bars in the left and right images represent 20 and 10 μm, respectively.

Fig. S5. The colocalization of SMNK-1 and SPE-18.

(A) SPE-18::mCherry was partially co-localized with SMNK-1::GFP in spermatocytes but not in spermatids. Scale: 5 μm.

(B) Loss of SPE-18 nearly had no effect on the formation of SMNK-1::GFP puncta in spermatocytes. The boxed areas in the left are magnified on the right. Scale bars in left and right panels represent 20 and 10 μm, respectively.

Fig. S6. The expression pattern of VHA-18.

(A) Sequence alignment of the VHA-18 amino acid and v-ATP H subunit in other species. From top to bottom: *Homo sapiens* ATP6V1H, *Mus musculus* ATP6V1H, *Drosophila melanogaster* VhaSFD, and *C. elegans* VHA-18.

(B) VHA-18::mCherry was expressed where spermatogenesis occurs in hermaphrodites and males. The bottom panels are the autofluorescence in control hermaphrodites and males. Scale: 50 μm.

(C) VHA-18::mCherrywas mainly expressed in the proximal terminal of male gonad indicated by the expression of GFP::NKB-2. Scale: 50 μm.

(D) VHA-18::mCherry was expressed and formed puncta associated with MOs (marked by GFP::SAC-1) in spermatocytes. Scale: 5 μm.

(E) VHA-18::mCherry puncta partially colocalizes with the MOs indicated by GFP::SAC-1 in the spermatids. Scale: 5 μm.

(F) The LysoTracker Red staining of dissected *vha-18* spermatids showed that some LysoTracker Red-stained structures are larger and scattered in the cell (middle), while in another case, LysoTracker Red only stains the outer space among the dark vacuoles (bottom), unlike the pattern observed in the control where LysoTracker Red-labeled puncta (MOs) lie underneath the PM (top).

(G) Quantification of the fluorescence intensity in the dashed lines shown in (F).

(H) Loss of SMNK-1 does not affect the morphology and the acidification of MOs in the spermatids. The LysoTracker staining shows no difference between spermatids of *him-5* and *smnk-1;him-5*. Scale: 5 μm.

Fig. S7. The VHA-18 is essential for FB-MO morphogenesis and protein sorting.

(A) EM images of spermatids from *vha-18;him-5* and *him-5* males. The red arrow in *vha-18* sperm indicates the structure resembling the lysosome. The blue arrow in *vha-18* sperm indicates the undissembled FB. The white dashed circle indicates the tiny vesicle closely adjacent to the large vesicle. Scale: 5 μm.

(B) Live cell imaging shows that spermatids from *vha-18;*GFP::NKB-2;H2B::mCherry contain many GFP-positive vesicles with more than one mCherry-labeled nucleus, while in control spermatids, the GFP localizes on the PM evenly, but not on internal organelle. Scale: 500 nm.

Video S1. The time-lapse analysis shows that early activated spermatozoa with punctate GFP::NKB-2 fluorescence are highly motile and move around in the seminal vesicle of control *swm-1;him-5* males (related to Fig. 2B).

Video S2. The time-lapse analysis shows the incompletely activated sperm with polarized GFP::NKB-2 puncta remain still in the seminal vesicle of *smnk-1;swm-1;him-5* males(related to Fig. 2B).

Figures

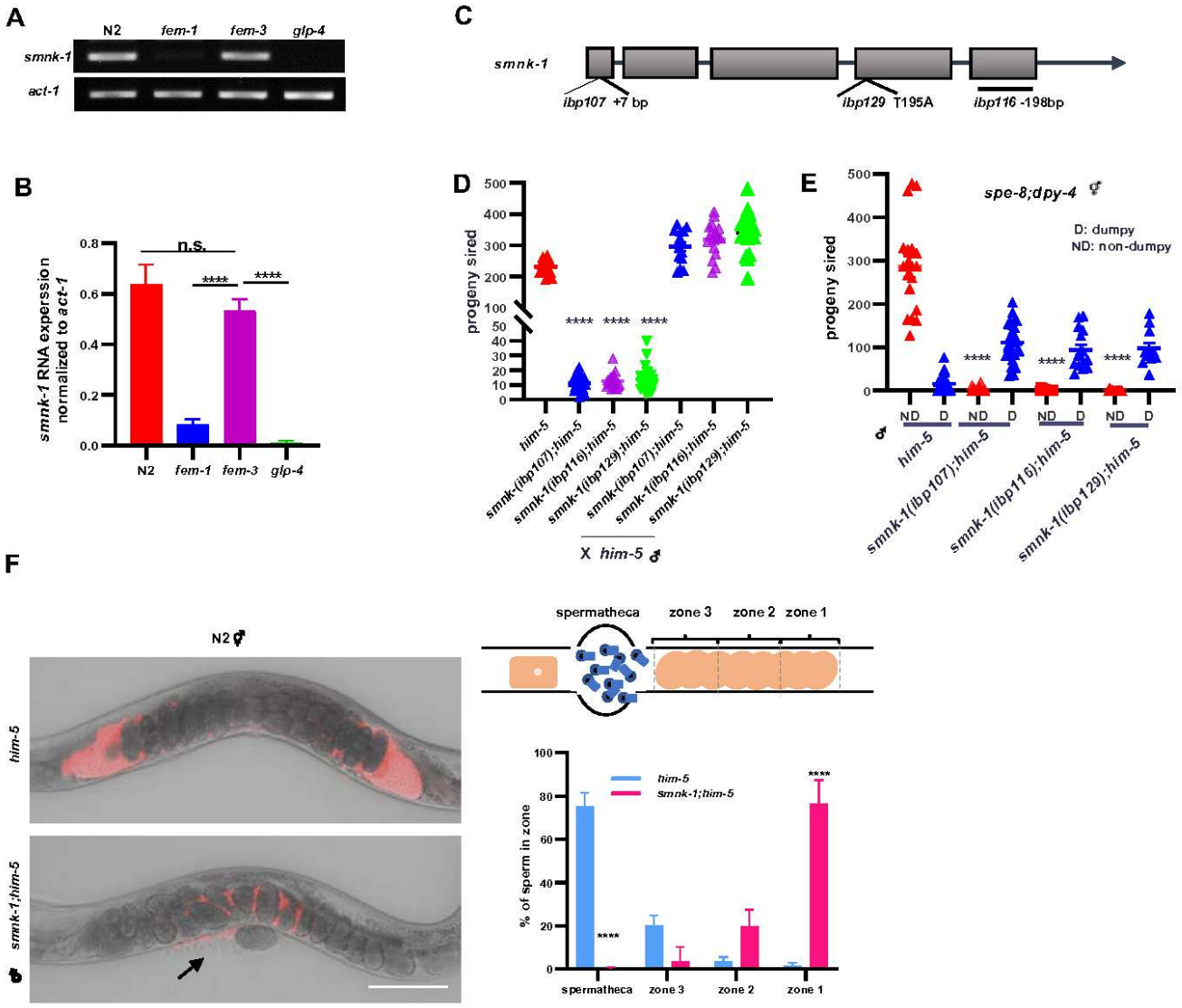

Figure 1

Casein-like kinase SMNK-1 is required for C. elegans fertility. (A) RT-PCR showed the relative expression of smnk-1 in N2 and fem-1 (hc17), fem-3(q96 gf) and glp-4(bn2) mutants, with act-1 serving as the control. fem-1 (hc17) and fem-3 (q96 gf) worms only produced oocytes and sperm, respectively, while glp-4(bn2) worms displayed defective germline development and do not produce either oocytes or sperm. (B) Quantification of relative smnk-1 expression shown in (A). values are means ± SEM. ****, P<0.0001. NS, not significant. (C) Genomic structure of smnk-1 gene. The boxes represent exons, and the solid lines represent introns. The mutations are labeled at their corresponding positions. smnk-1 (ibp107) is a frameshift mutation caused by a 7 bp insertion in the first exon. smnk-1(ibp129) is a point mutation at the putative active site residue T195; smnk-1(ibp116) is terminated at the 294th amino acid, thus a C-terminus deletion mutant. smnk-1(ibp129) and smnk-1(ibp116) are two alleles that might

affect kinase activity of SMNK-1. (D) The smnk-1 mutant hermaphrodites sired fewer progeny compared with control group, and the loss of fertility in smnk-1 hermaphrodite could be rescued by mating with him-5 males. (E) smnk-1 mutant males had impaired fertility. The number of cross progeny (ND, non-Dumpy) and self (D, Dumpy) progeny produced by spe-8;dpy-4 hermaphrodites was counted after mating with control him-5 or smnk-1; him-5 males. Values in (D) and (E) are presented as the mean ± SEM. ****$p < 0.0001$, in comparison to the control. (F) Sperm ejaculated from smnk-1(ibp107) males failed to migrate toward and accumulate in the spermatheca, unlike the behavior of sperm from control males. Males were stained with MitoTracker Red before mating with L4 virgin hermaphrodites. The arrow showed the MitoTracker Red-labeled male sperm from smnk-1;him-5 males located outside of the hermaphrodite uterus, which might be pushed out of the uterus during egg-laying. Scale: 50 μm.

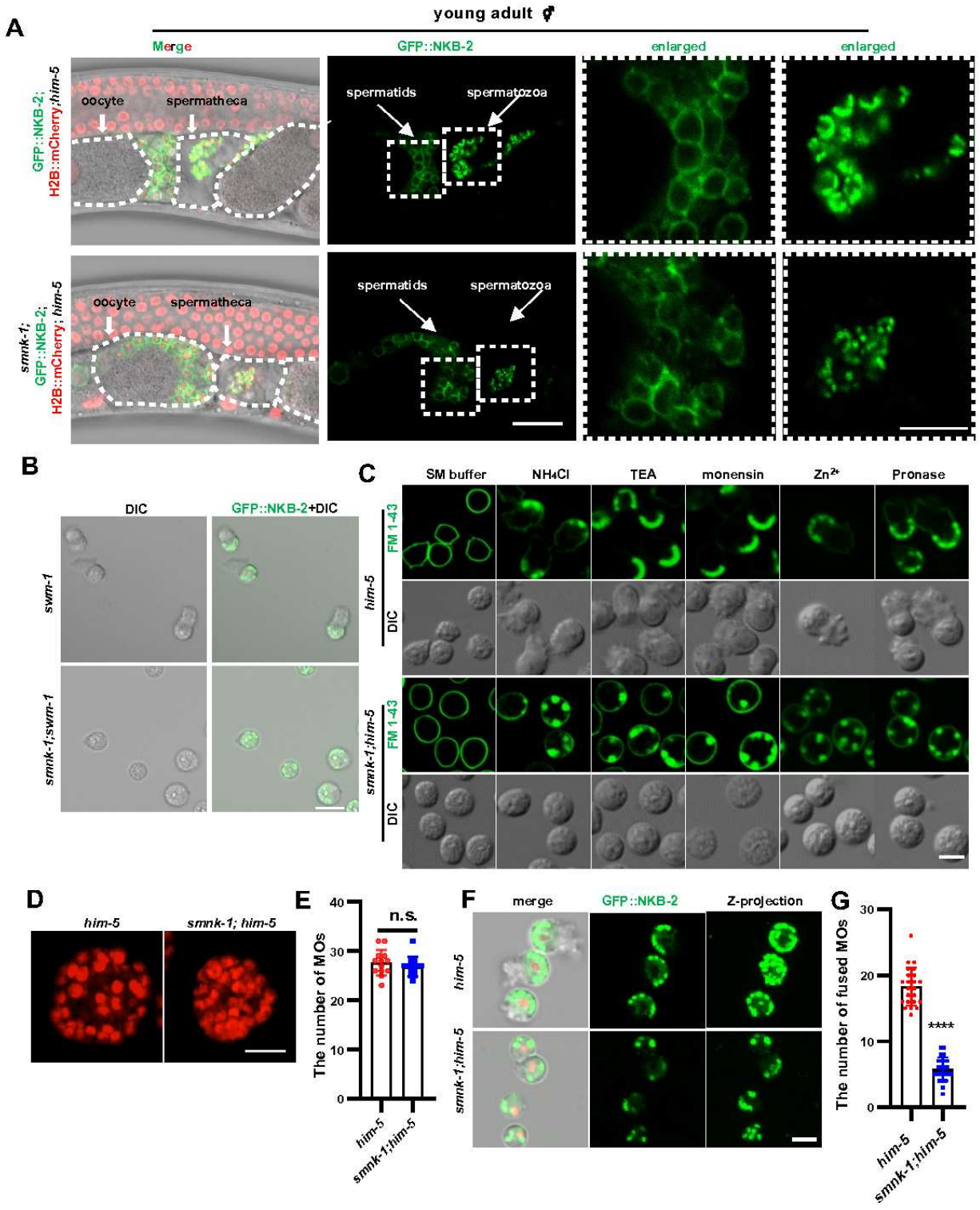

Figure 2

smnk-1 affects sperm activation and motility. (A) Loss of smnk-1 slightly affected hermaphrodite sperm activation, whichwas reflected by the number of GFP puncta on spermatozoa located in the spermatheca. Scale bars in left and right panels represent 20 and 10 μm, respectively. (B) The dissected sperm from male gonad of smnk-1;swm-1;gfp::nkb-2;him-5 and control group. In vivo activated smnk-1 sperm nearly had no pseudopod, though GFP::NKB-2 displaying a polarized pattern.

Scale: 5 μm. (C) smnk-1 affected sperm activation in vitro with extracellular sperm activators. SM represented the sperm medium, serving as the inactivated control; the known sperm activators, such as weak bases (NH4Cl and TEA), the proton carrier monensin, trace element Zn2+ , and Pronase, were used to trigger sperm activation. The MO fusions were indicated by the fluorescent puncta of membrane impermeable probe FM 1-43. Scale: 5 μm. (D) smnk-1 spermatids contained normal MOs as seen in control. The acidic MOs were labeled with LysoTracker Red. Scale: 5 μm. (E) Quantification of the number of the MOs indicated by LysoTracker Red shown in (D). (F) smnk-1 affected MO fusion and pseudopod extension when sperm were activated by Pronase. The fluorescent puncta of GFP::NKB-2 was used to indicate the fused MOs. Scale: 5 μm. (G) Quantification of the number of fused MOs indicated by GFP::NKB-2 puncta fluorescence in (F). Values in (E) and (G) are presented as the mean ± SEM. ****$p < 0.0001$. NS, not significant

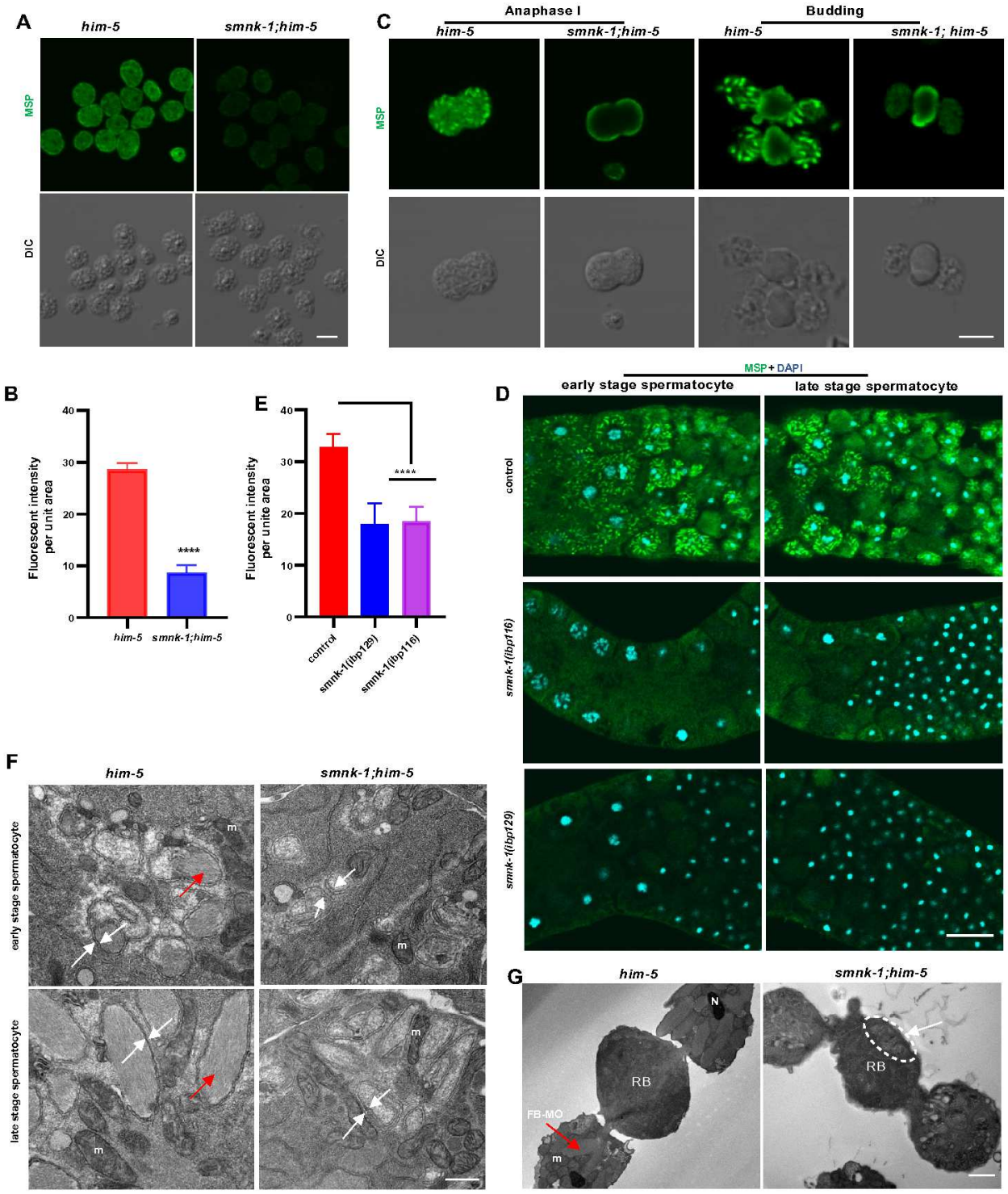

Figure 3

smnk-1 affects FB assembly in spermatocytes. (A) The anti-MSP immunofluorescence microscopy assay of spermatids from smnk-1(ibp107) and control males. Scale: 5 μm. (B) Quantification of MSP fluorescence shown in (A). Values are presented as the mean ± SEM. ****p < 0.0001. (C) The anti-MSP immunofluorescence microscopy assay of spermatocytes from smnk-1(ibp107) and control males in different stages. Green puncta observed in control cells indicate FBs. MSP fluorescence appeared

diffusive in the cortical area of smnk-1(ibp107) spermatocytes in anaphase I stage and in the cortex of RB during budding stage Scale: 5 μm. (D) The anti-MSP immunofluorescence microscopy assay of male gonads of smnk-1(ibp116), smnk-1(ibp129), and control wroms. MSP immunofluorescence appeared diffusive in smnk-1(ibp116) and smnk-1(ibp129) gonad, unlike the fluorescent puncta (FBs) observed in the control. Scale: 10 μm. (E) Quantification of MSP fluorescence shown in (D). Values are presented as the mean ± SEM. ****$p < 0.0001$. (F) EM images of spermatocytes from smnk-1(ibp107) and control males. White arrows: tubule-like MOs; red arrows in the left panels: FBs semi-enclosed by MOs; m: mitochondria. Scale: 500 nm. (G) EM images of sperm and RB in the budding stage from smnk-1(ibp107) and control males. Red arrows: FB-MO complex in control spermatids; The white dashed ellipse on the right showed the MO components, typically partitioned to spermatids, were lagged in RB in smnk-1;him-5. m: mitochondrion; N: nucleus. Scale: 1 μm.

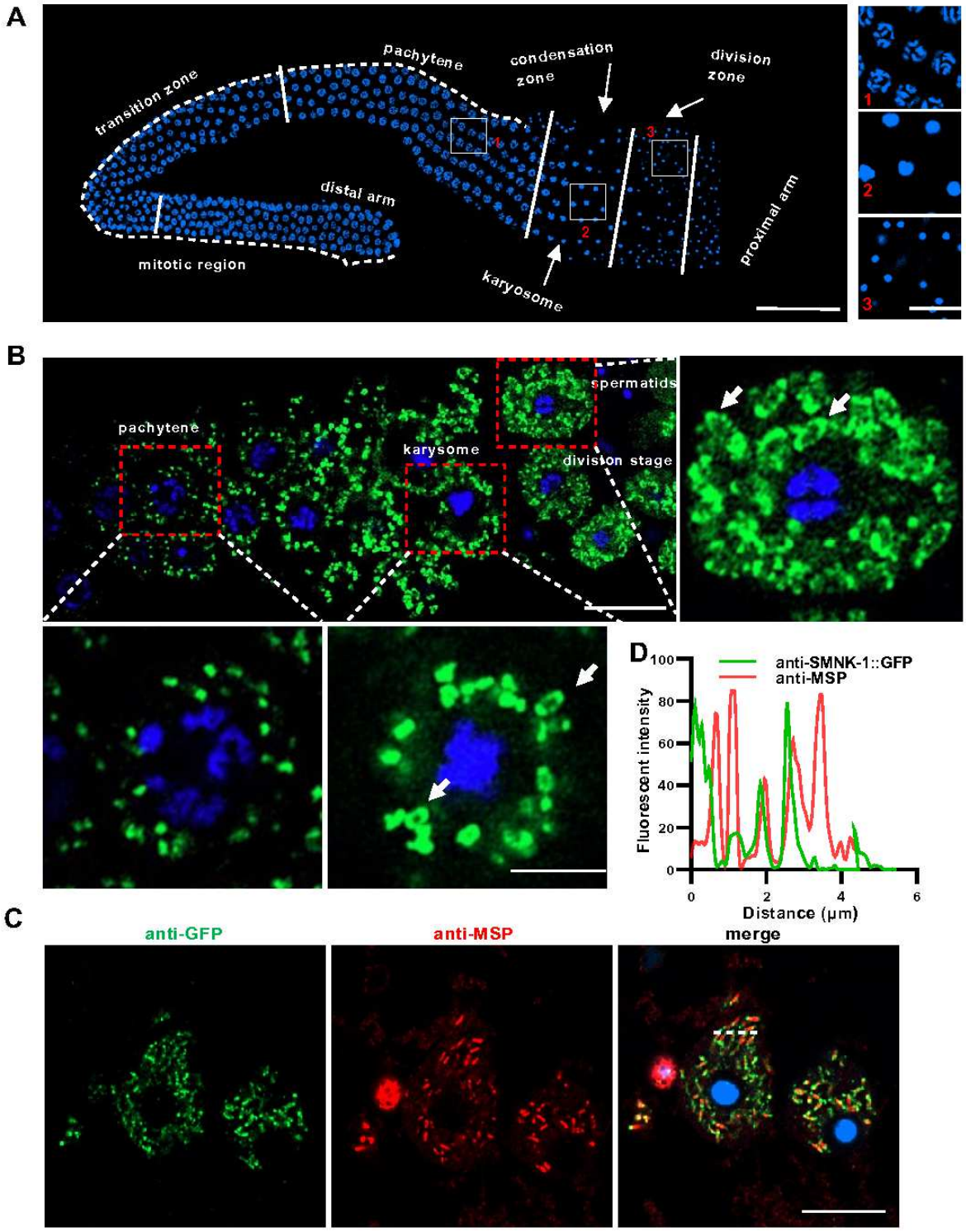

Figure 4

Punctate SMNK-1 is associated with FBs in spermatocytes. (A) The shape and size of the nuclei labeled by Hoechst illustrated the various developmental stages in the male gonad. Scale bars in the left and right panels represent 50 μm and 20 μm, respectively. (B) The expression and localization pattern of SMNK-1::GFP in the male gonad. The arrow indicated the boat-like structure of GFP puncta. The nuclei were labeled by Hoechst. Scale bars in the upper and lower panels represent 10 μm. (C)

Immunofluorescence microscopy assay showed that SMNK-1(green) was localized to the periphery of FBs (red) in meiotically dividing spermatocytes. The nuclei were labeled by DAPI. Scale: 10 μm. (D) Quantification of MSP and SMNK-1::GFP fluorescence in the dashed line shown in (C).

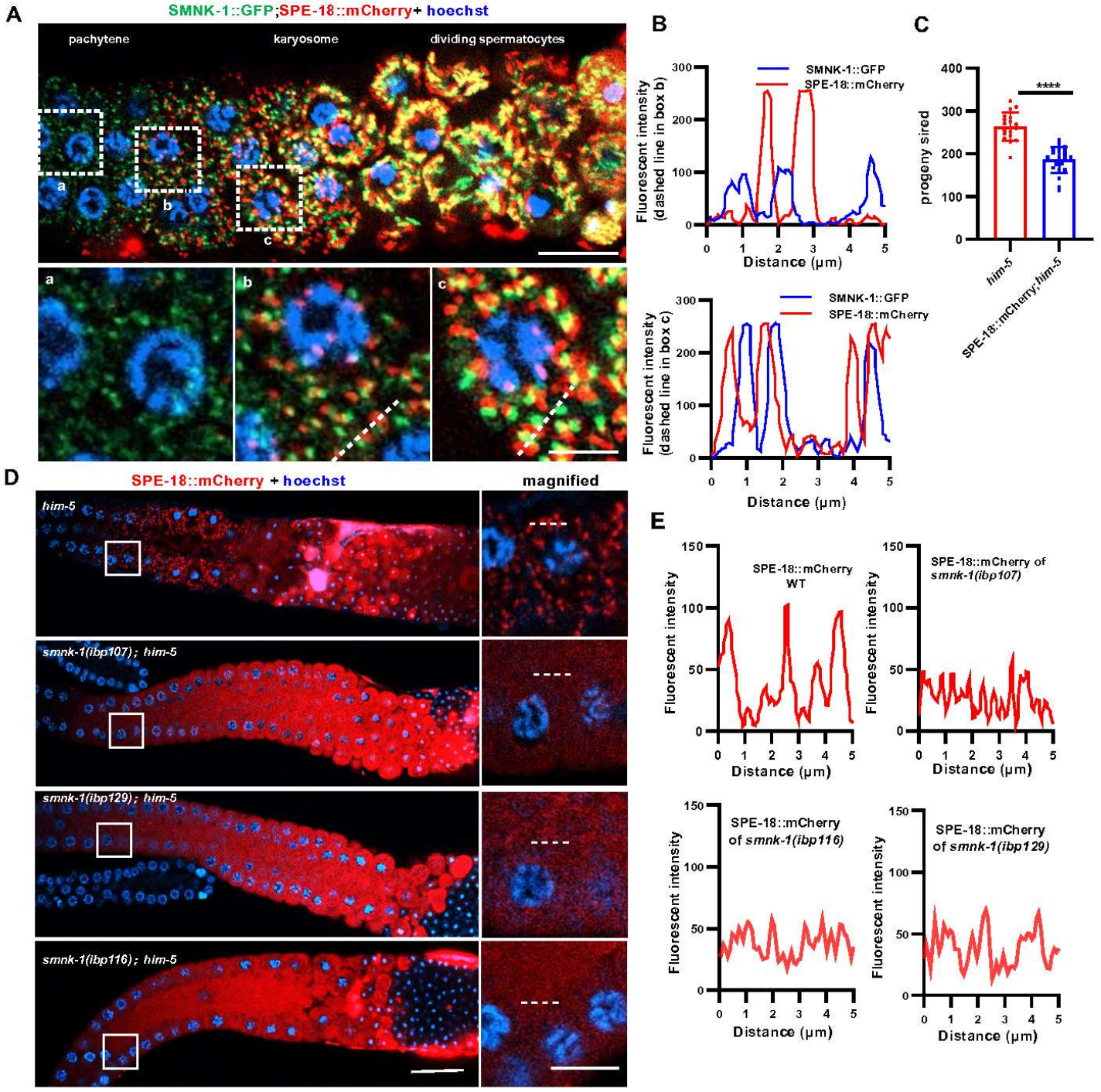

Figure 5

SMNK-1 functions upstream of SPE-18 and is required for recruiting SPE-18 to MOs. (A) Live-cell imaging of SMNK-1::GFP and SPE-18::mCherry in different stages of spermatogenesis indicated by the

nuclear size and structure. The appearance of SMNK-1::GFP occurred earlier than SPE-18::mCherry in the male gonad. The boxed areas in the upper panelwere magnified on the lower panels. Scale bars in the upper and lower panels represent 10 and 5 μm, respectively. (B) Quantification of SPE-18::mCherry and SMNK-1::GFP fluorescence intensity along the dashed line shown in (A).The upper and lower images correspond to the dashed lines in magnified b and c, respectively. (C) Inserting mCherry into the C-terminal of SPE-18 affected the fertility of hermaphrodites. values are presented as the mean ± SEM. ****$p < 0.0001$. (D) Loss of SMNK-1 affected the localization of SPE-18::mCherry during spermatogenesis. In the control, SPE-18::mCherry appeared as puncta, while in any of the three smnk-1 mutants, SPE-18::mCherry appeared diffusive in the cytoplasm. The boxed areas in the left are magnified on the right. Scale bars in left and right panels represent 20 and 10 μm, respectively. (E) Quantification of SPE-18::mCherry fluorescence intensity in the dashed lines shown in (D).

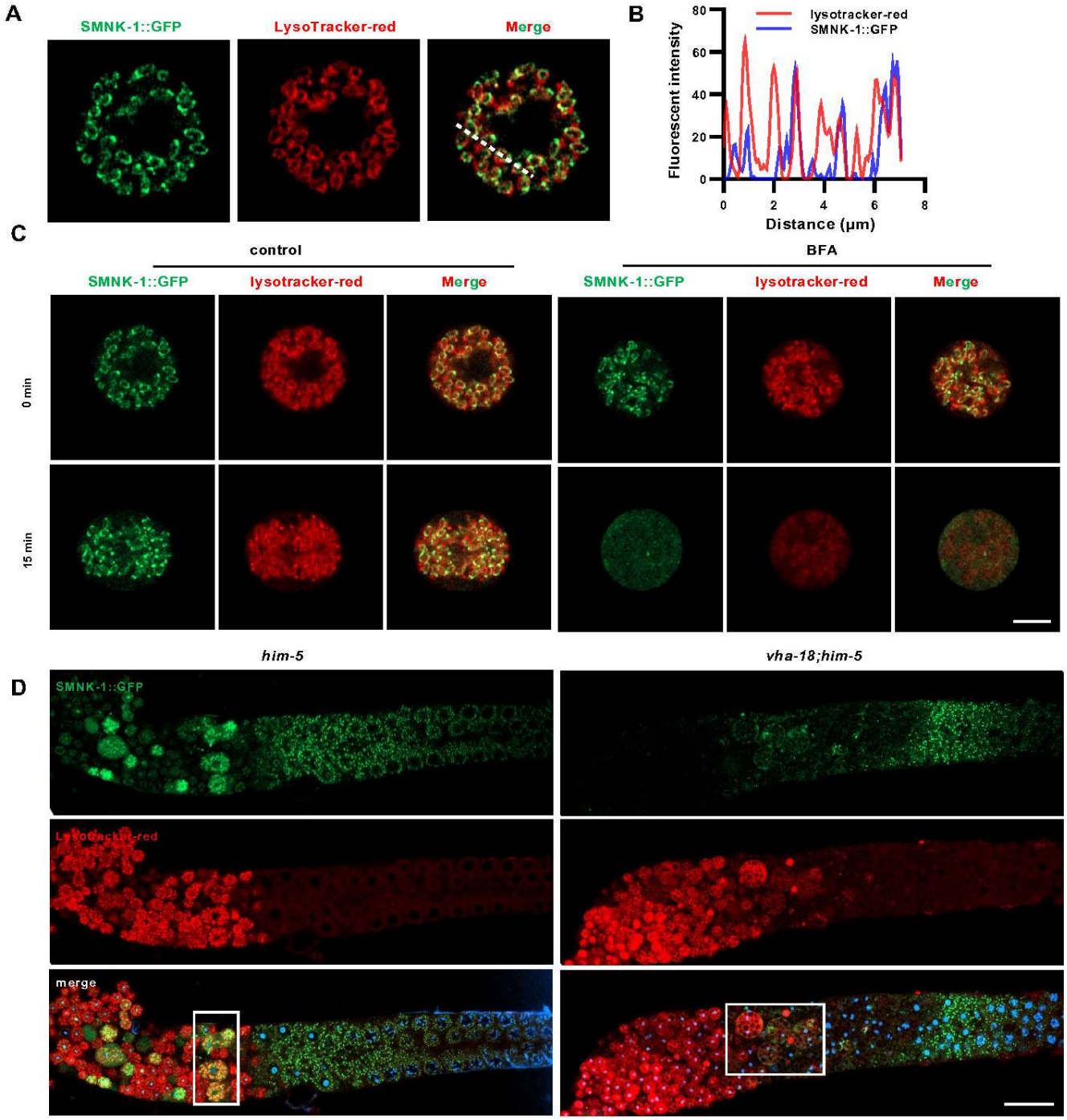

Figure 6

The acidification of MO lumen mediated by v-ATPase is required for FB-MO morphogenesis. (A) SMNK-1::GFP puncta were localized on the surface of acidic MOs probed by the LysoTracker Red. Scale: 5 μm. (B) Quantification of the SMNK-1::GFP fluorescence intensity in the dashed line shown in (A). (C) BFA treatment neutralized the lumen of MOs and caused the puncta of SMNK-1::GFP to diffuse in spermatocytes. Scale: 20 μm. (D) Loss of VHA-18 caused abnormal vacuoles scattered in the cytoplasm

and the failure of SMNK-1::GFP condensation in spermatocytes. Many big round and scattered vacuoles were not stained by LysoTracker Red in vha-18 spermatocyte. Meanwhile, the cytoplasmic space among vacuoles was stained heavily by LysoTracker Red, instead of the MOs lumen observed in the control. The fluorescence of SMNK-1::GFP appeared as puncta in the distal end, but decreased dramatically and failed to colocalize with LysoTracker Red in the area of spermatocyte in the proximal germline of vha-18 male. The white boxes indicate the spermatocytes undergoing meiotic divisions. Scale: 5 μm.

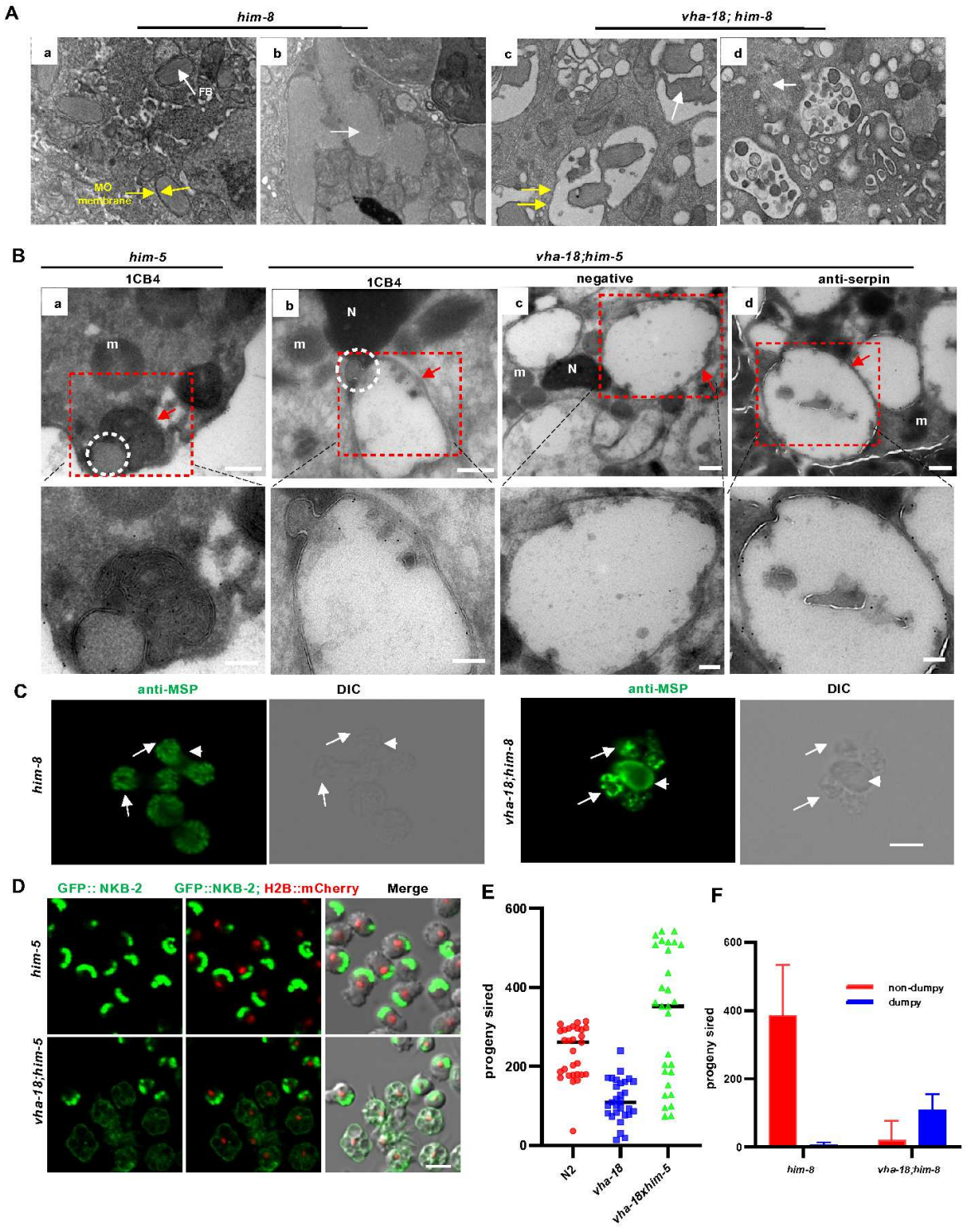

Figure 7

VHA-18 is required for MO-FB complex morphogenesis and male fertility. (A)EM images of spermatocytes in dissected male gonad from vha-18;him-8 or him-8 control. Many vesicles were observed in vha-18;him-8 spermatocytes. At the early stage of spermatocytes in vha-18;him-8 (Panel c), some assembled FBs were associated with the abnormal vesicles, unlike that seen in control where tubule-like MOs semi-enclose the FBs (Panels a and b); at the late stage of spermatocytes in vha-18;him-8 (Panel d), FBs expanded in both length and width were naked and not associated with the vacuoles. FB and MO membranes are labeled with white and yellow arrow, respectively. Scale: 500 nm. (B) Cryo-immuno EM analysis of vha-18;him-8 and him-8 control spermatocytes. Both MO membrane and vacuole membrane were recognized by 1CB4 (Panels a and b) and serpin antibody (Panel d). A smaller MO head (Panel b, the white dashed circle), and a swollen MO body (Panels b, c and d) could be observed in vha-18;him-8 spermatocytes, unlike that seen in control spermatocytes where normal sized MO head was connected via neck region to well-organized interrelated MO body (Panel a). The boxed areas in the upper panel were magnified on the lower panels. The antibody-conjugated colloidal gold particle can be distinctly observed in the bottom magnified panels a, b and d, but not panel c, which is the control without the primary antibody included. m: mitochondria; N: nucleus. The scale bar upper, 400 nm; the lower, 200 nm (C)VHA-18 was necessary for MSP sorting after anaphase II. Immunofluorescence microscopy assay with MSP antibody showed that though some big MSP puncta could be observed in the budding spermatids, dramatic amount of MSP was retained in the RB in vha-18;him-8. MSP puncta appeared relatively similar in size and number in the budding spermatids and barely visible in RBs in the control. The white arrow and arrowhead indicated the dividing spermatids and RB, respectively. Scale: 5 μm. (D)Loss of VHA-18 causeed sperm activation defects. TEA was used as extracellular agent to activate sperm. In the vha-18 mutant sperm, a diminished presence of fused MOs (as indicated by reduced GFP::NKB-2 puncta) and shorter pseudopods or spiky projections were observed in comparison to the control group. Scale: 5 μm. (E) Loss of VHA-18 affected hermaphrodite fertility. The reduced fertility of vha-18 mutant hermaphrodites was rescued by mating with him-5 males. (F) Loss of VHA-18 affected male fertility. The number of cross progeny (ND, non-dumpy) or self-progeny (D, dumpy) produced by spe-8;dpy-4 hermaphrodites are counted after mating with him-8 or vha-18;him-8 mutant males.

Supplementary Files

This is a list of supplementary files associated with this preprint. Click to download.

- table.pdf
- VideoS1.mp4
- VideoS2.mp4
- Supplementaryfigure.pdf